Remote Sensing of Environment 156 (2015) 247–263

Contents lists available at ScienceDirect

Remote Sensing of Environment

journal homepage: www.elsevier.com/locate/rse

Offshore wind climatology based on synergetic use of Envisat ASAR, ASCAT and QuikSCAT

Charlotte B. Hasager [a,*], Alexis Mouche [b], Merete Badger [a], Ferhat Bingöl [a], Ioanna Karagali [a], Tilly Driesenaar [c], Ad Stoffelen [c], Alfredo Peña [a], Nicolas Longépé [d]

[a] DTU Wind Energy, Technical University of Denmark, Frederiksborgvej 399, 4000 Roskilde, Denmark
[b] IFREMER, Pointe du Diable, 29280 Plouzané, France
[c] KNMI, Postbus 201, 3730AE, de Bilt, The Netherlands
[d] CLS, Bâtiment Le Ponant, Avenue La Pérouse, 29280 Plouzané, France

ARTICLE INFO

Article history:
Received 7 May 2014
Received in revised form 6 August 2014
Accepted 23 September 2014
Available online xxxx

Keywords:
Offshore wind
SAR
QuikSCAT
ASCAT
Wind energy
Resource
Northern Europe

ABSTRACT

The offshore wind climatology in the Northern European seas is analysed from ten years of Envisat synthetic aperture radar (SAR) images using a total of 9256 scenes, ten years of QuikSCAT and two years of ASCAT gridded ocean surface vector wind products and high-quality wind observations from four meteorological masts in the North Sea. The traditional method for assessment of the wind resource for wind energy application is through analysis of wind speed and wind direction observed during one or more years at a meteorological mast equipped with well-calibrated anemometers at several levels. The cost of such measurements is very high and therefore they are only sparsely available. An alternative method is the application of satellite remote sensing. Comparison of wind resource statistics from satellite products is presented and discussed including the uncertainty on the wind resource. The diurnal wind variability is found to be negligible at some location but up to 0.5 m s^{-1} at two sites. Synergetic use of observations from multiple satellites in different orbits provides wind observations at six times in the diurnal cycle and increases the number of observations. At Horns Rev M2, FINO1 and Greater Gabbard satellite and in situ collocated samples show differences in mean wind speed of −2%, −1% and 3%, respectively. At Egmond aan Zee the difference is 10%. It is most likely due to scatterometer data sampled further offshore than at the meteorological mast. Comparing energy density with all samples at Horns Rev M2 shows overestimation 7–19% and at FINO1 underestimation 2–5% but no clear conclusion can be drawn as the comparison data are not collocated. At eight new offshore wind farm areas in Denmark, the variability in mean energy density observed by SAR ranges from 347 W m^{-2} in Sejerøbugten to 514 W m^{-2} at Horns Rev 3. The spatial variability in the near-shore areas is much higher than at areas located further offshore.

1. Introduction

Offshore wind farms in Europe has grid connected capacity of 6.5 GW in 69 offshore wind farms, enough to provide 0.7% of the European Union's (EU) electricity according to the European Wind Energy Association (EWEA, 2013). The target on renewable energy production in EU 27 countries in 2020 is 20% and in 2030 is 27%. Offshore wind energy has the potential to supply a substantial share of this. In Asia offshore wind farms have been constructed in China, Japan, South Korea and Taiwan. For 2030 the targets on offshore wind power capacity are 30 GW in China, 2 GW in South Korea and 3 GW in Taiwan according to the Global Wind Energy Council (GWEC, 2013). In Japan 1 GW is planned for year 2020 at Fukushima (New Scientist, 2013). In Denmark a total of 1.5 GW in new offshore wind farms are being planned, some in near-shore areas according to the Danish Energy Agency (DEA, 2013). The United Kingdom Round 3 offshore wind farms will be located very far offshore (Crown Estate, 2013). The potential offshore wind energy in Europe is seven times Europe's energy demand as estimated by the European Environment Agency (EEA, 2009) and potential offshore wind energy near the United States could four times meet the energy demand in the USA according to the US Department of Energy (DOE, 2013).

Detailed knowledge on the potential wind resource is indispensable for planning each individual wind farm and to predict the expected annual energy production (AEP). AEP has to be known in order to secure finance. The more accurately the AEP, the less the financial cost will be (Petersen & Troen, 2012). The need to reduce cost on offshore wind farms is pressing (Fichtner, 2012). Offshore wind resources typically are estimated based on offshore meteorological observations and mesoscale modelling (Sempreviva, Barthelmie, & Pryor, 2008). The cost for offshore meteorological masts has increased dramatically in recent years (Henderson, Gandoin, Jiménez, Yendole, & Méchali, 2013). Wind

* Corresponding author. Tel.: +45 21327328.
E-mail address: cbha@dtu.dk (C.B. Hasager).

http://dx.doi.org/10.1016/j.rse.2014.09.030

profiling lidar on platforms appear a suitable alternative (Hasager et al., 2013) but often a platform is not available where the observations are most needed. Satellite remote sensing observations of ocean surface vector winds are available operationally and in archives, but not yet used to their full extent for wind energy resource assessment. The number of open seas measurements per year at each location from satellites is more than 4000 around Europe currently. The present study aims to progress satellite-based offshore wind resource mapping through synergetic use of SAR and scatterometer ocean surface wind observations.

Wind resource estimation using satellite SAR has been performed from ERS-1/-2 of the European Space Agency (ESA) in the North Sea (Hasager, Barthelmie, Christiansen, Nielsen, & Pryor, 2006; Hasager et al., 2005) but only few images were available. In the sea near Canada RADARSAT-1 SAR data from the Canadian Space Agency (CSA) were used for wind resource estimation based on few samples (Beaucage, Bernier, Lafrance, & Choisnard, 2008; Choisnard, Lafrance, & Bernier, 2004). The first study using Envisat ASAR from ESA was in the North Sea (Christiansen, Koch, Horstmann, Hasager, & Nielsen, 2006). The wind class methodology for offshore wind resource estimation based on SAR was suggested by (Badger, Badger, Nielsen, Hasager, & Peña, 2010) to compensate for the relatively low number of SAR samples; especially over sites outside Europe. In the Japanese seas (Takeyama, Ohsawa, Kozai, Hasager, & Badger, 2013a,b) and the Chinese seas (Chang et al., in review) SAR-based wind resource statistics were based on few Envisat scenes. The wind resource statistics in the Baltic Sea (Hasager, Badger, Peña, & Larsén, 2011) were based on around 1000 SAR-derived wind maps with the number of overlapping samples ranging from 250 to 450.

The advanced scatterometer ASCAT are on-board the Metop-A satellite of the European Organisation for the Exploitation of Meteorological Satellites (Eumetsat). Wind resources based on ASCAT ocean surface vector winds are studied here for the first time.

Ocean surface vector winds from the SeaWinds instrument on-board the QuikSCAT satellite from the National Aeronautics and Space Administration (NASA) have been used to study wind resources offshore Brazil (Pimenta, Kempton, & Garvine, 2008), in the Mediterranean Sea (Furevik, Sempreviva, Cavaleri, Lefèvre, & Transerici, 2011), the Northern European Seas (Karagali, Peña, Badger, & Hasager, 2014; Karagali et al., 2013), the seas near China (Jiang, Zhuang, Huang, Wang, & Fu, 2013), the Great Lakes (Nghiem, Leshkevich, & Stiles, 2004) and globally (Capps & Zender, 2010; Liu, Tang, & Xie, 2008).

Sun-synchronous polar-orbiting satellites observe locally at fixed hours in ascending and descending swaths. Thus if significant diurnal wind variations occur at a site, the wind resource estimation may be biased when using wind observations from only one satellite. Diurnal mean wind variations are typically a few tenth of a metre per second in open sea, but much larger in coastal areas with land–sea breezes and horizontal advection (Ricciardulli & Wentz, 2013). Combining wind observations from several satellites with different local equatorial crossing time may limit the problem. At the same time the total number of samples will increase and the statistical uncertainty decreases through synergetic use of satellite wind observations from multiple platforms.

The hypothesis of this study is that additional usage of space-borne SAR data combined with QuikSCAT and ASCAT can increase the accuracy of the offshore wind resource estimates. In this study Envisat ASAR images are processed from raw data to 10 m wind speed using three geophysical model functions (GMFs) and the results are tested against the high-quality in-situ wind data. Maps of wind resource statistics from the Northern European Seas (50°N to 64°N and 6°E to 22°W) are presented from each of the satellite sources, Envisat ASAR, ASCAT and QuikSCAT, and also combined. The diurnal wind variation is investigated and the synergetic use of wind observations from all three sensors is demonstrated. The combined wind resource statistics are compared to in situ results at two sites. This is novel and progress beyond state of the art in offshore satellite-based wind resource mapping. Special attention is given to the new near-shore wind farm areas in Denmark where the variability in the horizontal wind speed gradient is expected to be large due to coastal effects (Barthelmie et al., 2007). Only SAR is able to cover the near-shore areas. One advantage of satellite observations is that most seas worldwide are covered, thus the methodology is applicable anywhere.

The paper is structured with the material and methods described in Section 2. Section 3 contains comparison results between in situ and satellite winds and wind resource statistics. The discussion and conclusions are presented in Sections 4 and 5, respectively.

2. Material and methods

2.1. Envisat ASAR, ASCAT and QuikSCAT

The present analysis is based on SAR data from the Envisat 10-year archive from 2002 to 2012, and gridded ocean surface vector wind products from the 2-year archive of ASCAT from 2007 to 2008 and the 10-year archive of QuikSCAT from 1999 to 2009.

Common to the three satellite instruments being used in this work is that they are active sensors based on microwave technology. One of the advantages of radar is that observations are obtained in all weather conditions, day and night. Thus all types of offshore wind conditions may potentially be observed. Each retrieved wind field is a snap-shot of the conditions at the time of observation. All instruments are on-board sun-synchronous satellite platforms and this gives a regular time of observation in ascending and descending mode.

The observations of ocean surface winds from all instruments are physically related to the observed microwave backscatter that is a function of the short capillary-gravity waves. These short waves are primarily being generated by the instantaneous wind field. It has been found that empirical functions are robust for retrieval of the surface ocean winds at 10 m above sea level. The empirical GMFs used to retrieve satellite winds are based mainly on moored buoy wind data and weather model results. The accuracy of the satellite-based wind observations has been investigated by comparing them to continuously monitored, offshore moored buoy wind observations that are also being used for climate data records.

Land surfaces, islands and even smaller units such as ships, wind turbines and other hard targets affect the radar observations. Dependent upon the spatial scale covered these hard targets give higher backscatter most obviously noted for low winds. The extremely high backscatter values are generally rejected by wind retrieval quality control at low winds for scatterometer using maximum likelihood estimation. For higher winds speeds the quality control for hard targets is less obvious. Thus even with the quality control included hard targets may bias the ocean wind speed results positively, i.e., the sampled wind speeds may be higher than the true time average wind speed. Observations with both high and low spatial resolutions are affected.

Envisat ASAR provides images at various resolutions. In the present work only wide swath mode (WSM) is used. The resolution is around 150 m but in order to provide ocean winds, it is necessary to average to around 1 km to reduce the inherent speckle noise, a random phenomenon in radar, and also eliminate effects of tilt and modulation error from longer waves, before wind inversion. SAR-based ocean surface wind retrieval is described in (Dagestad et al., 2013) and references therein. Wind direction needs to be known a priori for wind speed retrieval from SAR at the same resolution as the wind speed retrieval is performed. Wind direction is typically used from atmospheric models where the wind direction is interpolated in space and time to the SAR data, but lacks similar spatial resolution and accuracy (Monaldo, Thompson, Beal, Pichel, & Clemente-Colón, 2001). Other options for obtaining wind directions are: wind streak analysis (Furevik, Johannessen, & Sandvik, 2002; Gerling, 1986; Koch, 2004; Lehner, Horstmann, Koch, & Rosenthal, 1998) or the Doppler shift in SAR data (Mouche et al., 2012), from scatterometer (Monaldo, Thompson, Pichel, & Clemente-Colon, 2004) and from in-situ measurements (Christiansen et al., 2006; Hasager

et al., 2005). Each WSM image has a swath of 400 km. It is possible to map a certain point at mid-latitude (55°N) around 15 times per month. Thus the spatial resolution is high but the temporal resolution is low. The near-shore coastal zone can be observed to around 1 km distance. The GMFs valid for open-ocean may not be fully valid in coastal zones with short fetch but alternatives are not available. Envisat ASAR is working at C-band (5.3 GHz) which is not much affected by rain.

ASCAT and QuikSCAT are in mission with the specific goal of observing the equivalent-neutral surface ocean vector winds. These are 10 m vector winds computed from the surface roughness conditions under neutral atmospheric stratification. This facilitates comparison with buoy and numerical weather prediction model data, while, at the same time, does not introduce a dependency of backscatter-inferred winds on atmospheric stability assumptions. The required local wind vector precision and accuracy are, respectively, 3.0 m s^{-1} and 0.5 m s^{-1} for ASCAT and QuikSCAT, but validation studies by for example triple collocation show that KNMI products have about 1.0 m s^{-1} wind vector precision and 1% accuracy (Vogelzang, Stoffelen, Verhoef, & Figa-Saldana, 2011). Areas with sea ice are flagged out before wind inversion for ASCAT and QuikSCAT.

ASCAT-A was launched in 2006 and continues in operation in tandem with ASCAT-B, launched in 2012. ASCAT is also working at C-band (5.3 GHz). The ASCAT CMOD5N GMF used in the present analysis is based on triple collocation analysis of neutral winds (CMOD5N, 2013; Hersbach, 2010; Portabella & Stoffelen, 2009). Scatterometer winds are operationally monitored, undergo advanced calibration and validation by triple collocation since many years (e.g., Stoffelen, 1998; Vogelzang et al., 2011) and products from different providers are compared (e.g., Ebuchi, 2013; Stoffelen, Vogelzang, & Verhoef, 2010) from sources such as Eumetsat Ocean and Sea Ice Satellite Application Facility (OSI SAF) at the Royal Netherlands Meteorological Institute (KNMI) (OSI SAF, 2014), the National Oceanic and Atmospheric Administration (NOAA, 2014), and Remote Sensing Systems (RSS, 2014).

A single ASCAT provides ocean surface vector winds in two swaths of 550 km and thus maps all locations at 55°N around 40 times per month. The two ASCAT instruments (ASCAT-A and ASCAT-B) will operate in tandem in the future and provide improved coverage, around 80 observations per month at 55°N. The coastal wind product has a resolution of 12.5 km and can map as close as 10 km from the coast (Verhoef & Stoffelen, 2013). In the present study is used ASCAT-A observations from 2007 and 2008 at 12.5 km by 12.5 km spatial grid from the catalogue MyOcean (MyOcean Catalogue, 2014).

The QuikSCAT observations are collected from 1999 to 2009. Multiple radar backscatter measurements over an area are obtained from different viewing angles and are organized to wind vector cells. The measurements are fed in the GMF maximum likelihood estimation inversion and multiple sets of wind speed and direction estimates are produced. Through a spatial filtering method the final ambiguity removal is done. The physical parameter is the equivalent neutral wind at 10 m above the surface (Liu & Tang, 1996). In the coastal zone winds cannot be obtained from QuikSCAT observations. QuikSCAT operated at 13.4 GHz (Ku-band) which is sensitive to rain. Rain scatters and attenuates the radar signal and modifies the ocean surface. It has been found that, on average, rain contaminated scatterometer winds are biased towards higher wind speeds (Hilburn, Wentz, Smith, & Ashcroft, 2006).

The QuikSCAT satellite swath was 1800 km wide and most of the entire ocean was mapped twice per day. At 55°N the observational frequency is over 60 per month. The spatial grid is 25 km. The spatial resolution is low but the temporal resolution is high. In the present study QuikSCAT JPL (v4) GMF Ku-2011 is used (Ricciardulli & Wentz, 2011, 2013) and data are the gridded wind product at grid resolution 25 km by 25 km from Remote Sensing Systems (RSS, 2014). The wind products contain rain-flags and users can discard these data. This is done in the present analysis.

2.2. Satellite data extraction and processing

In this study Envisat SAR images are processed from raw data to 10 m wind speed. The SAR data are calibrated and SAR-derived winds are retrieved using three GMFs: CMOD-IFR2 (Quilfen, Chapron, Elfouhaily, Katsaros, & Tournadre, 1998), CMOD5 (Hersbach, Stoffelen, & de Haan, 2007) and CMOD5N (CMOD5N, 2013). The spatial grid is 1 km by 1 km.

For SAR wind retrieval it has been suggested to remove hard targets using SAR-based ship detection methodology to identify ships and then omit these values before wind inversion (Longépé, Hajduch, Pelich, Habonneau, & Lebras, 2013). This pre-processing has been applied at very high resolution (75 m) to filter out non-geophysical backscatter contributions before deriving the wind at kilometre scale. In addition, SAR wind measurements are considered as valid when they are more than 1000 m offshore to avoid contamination by the coast in the backscatter.

Envisat SAR scenes covering the Baltic, Irish and North Sea were retrieved and processed. We were fortunate to obtain 9256 unique Envisat ASAR scenes, hereof 4665 from ascending (northbound) passes usually observed within the local overpass time interval around 21:19 to 21:47 UTC, and 4591 scenes from descending (southbound) passes in the time interval around 09:53 to 10:23 UTC. The ascending and descending orientation of the wind maps is slightly, but opposite, tilted due to the near-polar orbital geometry. The track angle was typically −14° and −166° for ascending and descending passes, respectively. This gives rise to a typical harlequin checkered pattern in the number of overlapping observations. The number of overlapping scenes ranges from approximately 200 for areas northwest of the UK to 1400 for parts of the Norwegian coastal seas. The study area covers from latitude 50° to 64°N and longitude 6°W to 22°E (see Fig. 7).

Ocean winds may exhibit seasonal and diurnal variations. Therefore observations were collected during all months and in ascending and descending modes. The data are listed in Table 1. Since 2006 we mainly use the ESA rolling archive.

CLS developed a reprocessing chain able to massively process images using the method described in (Portabella, Stoffelen, & Johannessen, 2002). This methodology was revisited by Kerbaol (2007) to reduce the computational cost. CLS used the latest version of the algorithm for the reprocessing. For HH data the polarization ratio with both incidence angle and wind direction relative to the radar look angle is used (Mouche, Hauser, Daloze, & Guerin, 2005). At CLS the European Centre for Medium-range Weather Forecasts (ECMWF) atmospheric model wind directions (Brown et al., 2005; Vogelzang et al., 2011) were used in the backscatter-to-wind inversion scheme. Ancillary data are given by ECMWF at spatial grid of 0.125° (or 0.5° when 0.125° is not available) and 3-hourly (or 6-hourly, when 3-hourly is not available). The data are interpolated in space to the SAR scenes before wind inversion. The collocation in time is so that the closest ECMWF output in time is used. To omit areas with sea ice before wind inversion the mask by OSI SAF is applied. Fig. 1 shows a wind map processed by CLS.

ASCAT ocean surface vector winds were collected in gridded version by KNMI. KNMI produces since November 2009 the coastal ASCAT scatterometer swath product within the context of the Eumetsat OSI SAF. This product consists of measurements of wind speed and direction (equivalent neutral at 10 m) within a wind vector cell of size 12.5 km (ASCAT Wind Product User Manual, 2012) oriented according to the satellite swath. In the context of (MyOcean Catalogue, 2014) a version of this product is produced on a fixed geographical grid since the beginning of 2012, the MyOcean L3 Global wind product.

For the period of 1 June 2007 to 31 December 2008 the Full Resolution product of ASCAT was reprocessed into the ASCAT coastal L2 product (Verhoef, Vogelsang, Verspeek, & Stoffelsen, 2010; Verspeek, Portabella, Stoffelen, & Verhoef, 2011) on a grid of 12.5 km. The input ASCAT Full Resolution data was retrieved from the NOAA CLASS archive. The reprocessing was done using the ASCAT Wind Data Processor package version 2.1 of the Eumetsat Numerical Weather Prediction (NWP)

Table 1
Number of Envisat ASAR, ASCAT and QuikSCAT (QSCAT) wind maps in total, in ascending (asc.) and descending (des.) mode and per month. Approximate overpass time at 55°N in UTC.

	Total	Asc.	Des.	1	2	3	4	5	6	7	8	9	10	11	12
ASAR	9256	4665	4591	887	775	932	742	777	641	690	772	751	784	729	776
ASCAT	1141	569	572	58	58	60	58	62	120	117	124	116	124	120	124
QSCAT	7282	3641	3641	310	283	309	300	308	300	308	310	299	310	294	310

	Ascending time [time range]	Descending time [time range]
ASAR	21:30 [21:17; 21:47]	10:30 [09:53; 10:23]
ASCAT	21:00 [19:48; 21:28]	10:00 [09:20; 10:59]
QSCAT	06:00 [04:18; 06:06]	18:00 [17:48; 19:42]

SAF (Verhoef et al., 2010). This product was then gridded into the L3 ASCAT 12.5 km product (MyOcean Product User Manual, 2012) for the study area. The gridding is done using the Gouraud shading technique resulting in an ascending and a descending file each day. Only wind vector cells that have successfully passed KNMI quality control are used in the gridding.

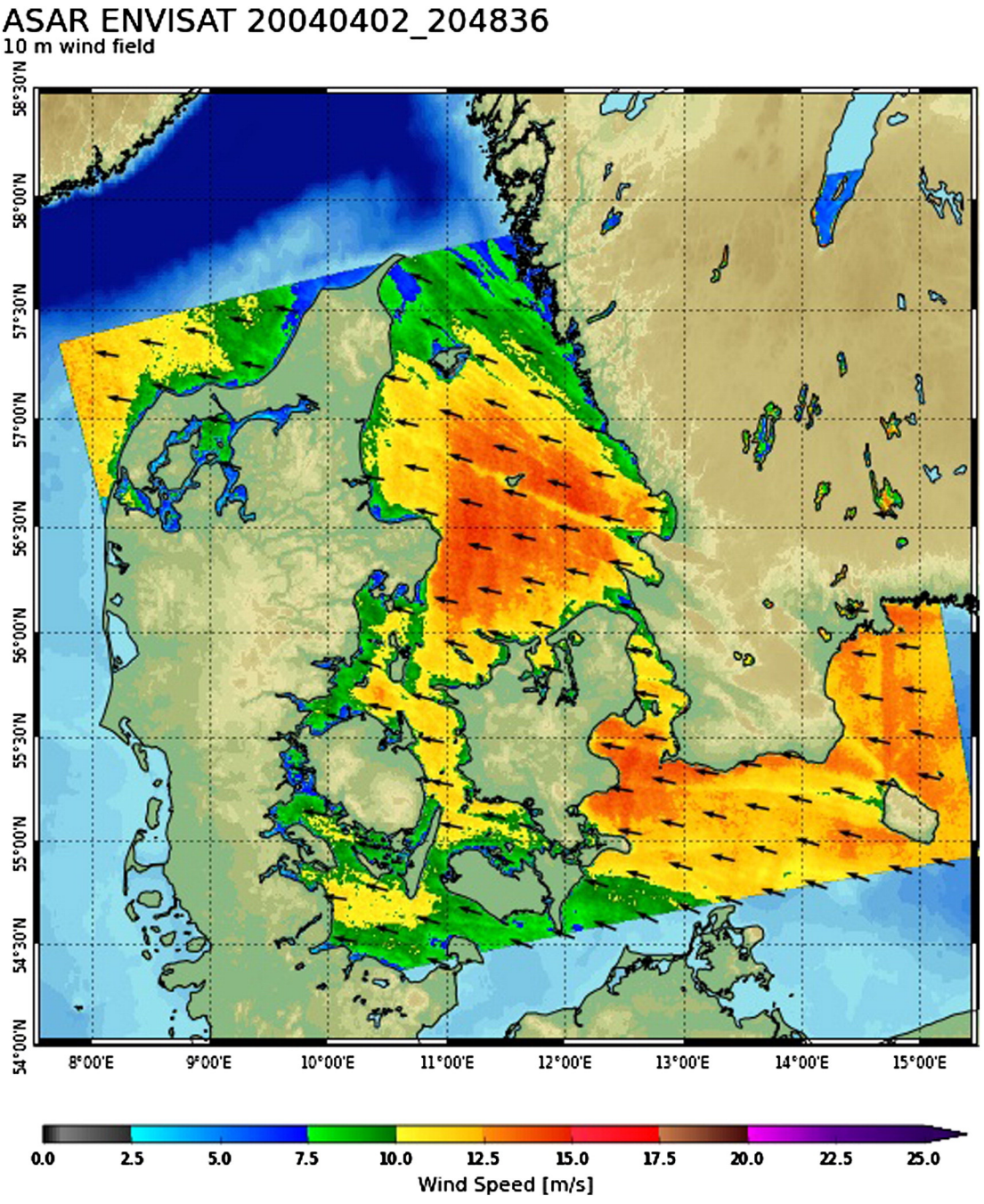

Fig. 1. Wind map from Envisat ASAR from 2 April 2004 at 20:49 UTC covering the Danish Seas. Processed at CLS.

The descending ASCAT swaths pass the North Sea each morning around 09:20 to 10:59 UTC and the ascending swaths pass around 19:48 to 21:28 UTC. In Table 1 the distribution of data used from ASCAT in total, per month and ascending and descending swaths are listed. The number of overlapping wind maps is shown in Fig. 7 and an example of an ASCAT wind map is shown in Fig. 2. It is observed on 01.10.2008 at around 10:30 UTC and show high winds near England and low winds near Norway.

QuikSCAT ocean surface vector winds were collected in gridded version from RSS in v4 (RSS, 2014). In the present study rain-contaminated winds were excluded from the analysis following the RSS rain flag. The ascending QuikSCAT swaths pass the North Sea each morning around 04:18 to 06:06 UTC and the descending swaths pass around 17:48 to 19:42 UTC. In Table 1 the QuikSCAT data used in the study are listed including the total number, the ascending and descending swaths and the number of samples per month. The number of overlapping wind maps is shown in Fig. 7. Fig. 3 shows an example of a QuikSCAT wind map. The wind map is from 01.01.2009 observed around 06:00 UTC. The winds east of England are low whereas the winds near Norway are high. In the Baltic Sea wind observations are only provided in the central part of the basin due to sea ice flag in the coastal and northern parts.

2.3. Meteorological data, diurnal wind speed variation and deriving 10 m wind speed

Meteorological observations from four tall masts in the North Sea are used for comparison analysis to estimate the local accuracy. The satellite data represents area-mean winds, while the masts represent local winds. The representation of local accuracy thus depends on local wind variability. Vogelzang et al. (2011) find buoy vector errors around 2 m s^{-1} on the scatterometer scale; locally the buoy errors are below 0.5 m s^{-1} root mean square error (RMSE). Thus the mast data are not directly useful to test satellite wind quality but is useful for checking the local representation for wind energy applications.

The data quality is high at the meteorological masts as these are established for wind resource estimation. For the individual wind speed sensors accuracy is around 0.2 m s^{-1} but flow distortion due to masts, booms, etc. has to be checked. Information on the observations at the meteorological masts is given in Table 2. Also the start of the construction of the nearby offshore wind farms and the time of first power generation is listed. During the construction phase many ships are in the area and reflections from ships, foundations and wind turbines may impact the satellite observations. Once the power generation starts the wind farm wake may influence the meteorological observations for certain wind directions. The distance to nearest coastlines is listed.

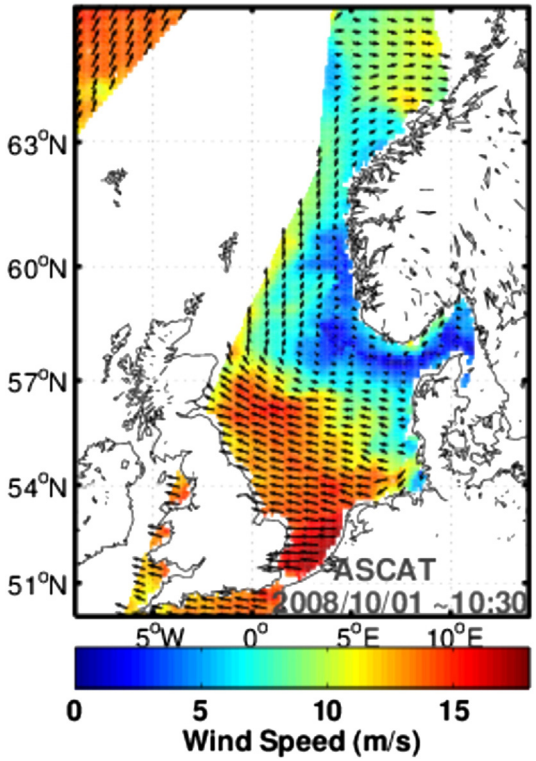

Fig. 2. Wind map from ASCAT.

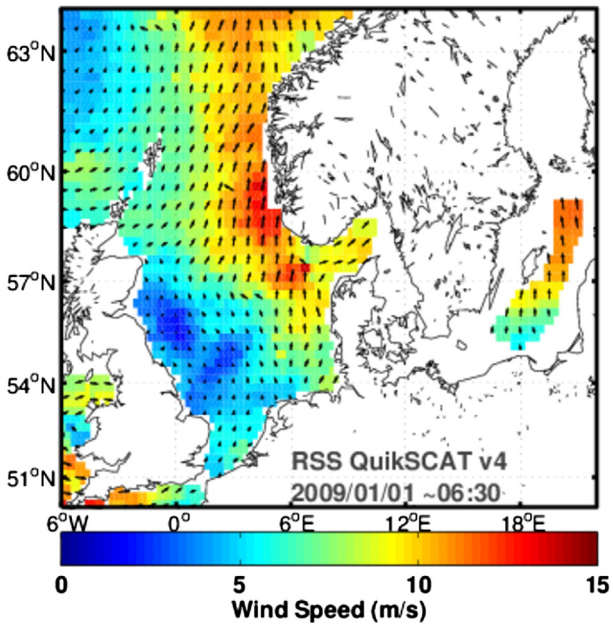

Fig. 3. Wind map from QuikSCAT.

The Egmond aan Zee offshore wind farm was constructed in April 2006 to 2007 with first power generation in October 2006 (commissioned in 2007) and consists of 36 3 MW turbines within an area of 27 km^2. The free stream sector from the meteorological mast is from 135° to 315° and with possible influence of wind farm wake in the remaining sector (e.g. Sathe, Gryning, & Peña, 2011).

The alpha ventus offshore wind farm was constructed from August 2007 to 2010 with first power generation in August 2009 (commissioned 2010) and consists of 12 5 MW turbines covering 4 km^2. The FINO1 meteorological mast is located west of the wind farm and has free sector from 180° to 360° and wake influence from 0° to 180°.

The Greater Gabbard offshore wind farm was constructed in September 2009 to 2012 with first power production in March 2011 (commissioned 2012) and consists of 140 3.6 MW turbines covering 147 km^2. The meteorological mast data are not influence by wind farm wakes.

The Horns Rev 1 offshore wind farm was constructed in February 2002 and first power production was in July 2002 (commissioned 2002). It consists of 160 2 MW turbines and cover an area of 20 km^2. The free stream directions from Mast 2 (M2) are from 0° to 90° and from180° to 360°, so only in the 90° to 180° sector wind farm wake influences are possible. The Horns Rev 2 offshore wind farm located north of M2 could not induce wind farm wake as the construction started in May 2008 and first power generation is from March 2009.

The map in Fig. 4 shows the location of the meteorological masts and the eight new offshore wind farm areas in Denmark (cf. Section 3.4).

The average wind speed during 24 h at the four masts is investigated for the existence of strong diurnal winds, in which case satellite winds may not be fully representative of average daily values due to the limited temporal coverage. Using satellite data at different observing times may limit the problem. The result is shown in Fig. 5. The nearest

Table 2
Meteorological masts and distance to nearest coastline: period of observation, heights of observations of wind speed (WS), pressure (P), wind direction (WD), temperature (T) and relative humidity (RH) above mean sea level in metres (m). The start of nearby wind farm construction and first wind turbine power generation (wake).

Meteorological mast	Period…	Height (m)	Construction	Wake…
Egmond aan Zee (15 km to coast of the Netherlands)	Jul.2005 Dec. 2008	WS: 21, 70, 116 P: 20 WD: 21, 70, 116 T: −3.8, 21, 70, 116 RH: 30, 70, 99	Apr. 2006	Oct. 2007
FINO1 (45 km north of island Borkum, 56 km to coast of Germany)	Aug. 2003 Apr. 2010	WS: 33, 40, 50, 80, 90, 100 P: 20, 90 WD: 33, 40, 50, 60, 80 T: −3, 30, 40, 50, 70, 100 RH:33, 50, 90	Aug.2007	Aug. 2009
Greater Gabbard (32 km to coast of UK, 100 km to coast of Belgium)	Jan.2006 Jul.2010	WS: 42.5, 52.5, 72.5, 82.5, 86.5 P: 84,5 WD:62.5 T:84.5 RH:38.5	Sep. 2009	Mar. 2011
Horns Rev M2 (17 km to coast of Denmark)	Jan.2003 Dec. 2008	WS: 15, 30, 45, 62 WD: 28, 43, 60 T: −4, 13, 55 RH: 13 P:55	Feb. 2002	Jul. 2002

observation heights to 10 m above mean sea level (amsl) are chosen. The graph shows negligible diurnal wind speed variations at FINO1 and Horns Rev M2 and up to 0.5 m s^{-1} at Egmond aan Zee and Greater Gabbard. The approximate overpass times of the satellites are indicated. FINO1 is located far offshore and M2 is dominated by westerly winds (cf. Section 3.3 on wind roses) whereas Egmond aan Zee and Greater Gabbard appears to be more influenced by coastal winds. The proximity to coastlines and dominant wind directions influence the average diurnal wind speed variation.

Satellite-based winds are valid at 10 m above mean sea level thus it is necessary to extrapolate the winds observed at higher levels to 10 m before comparing the meteorological mast data and satellite data. The extrapolation done in this study is described below.

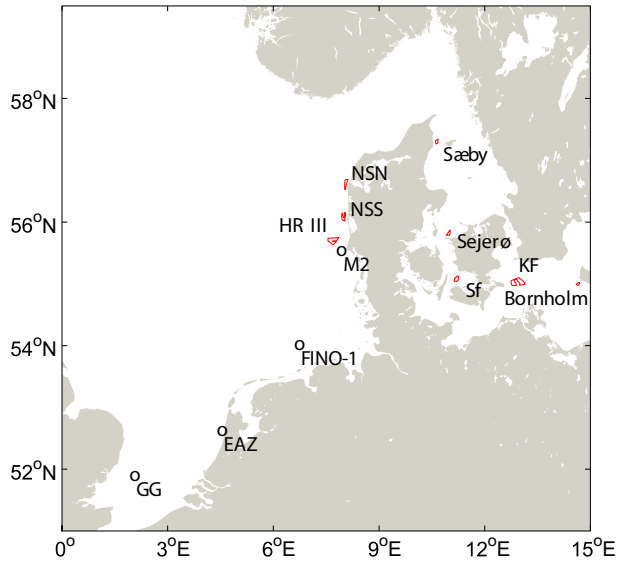

Fig. 4. The locations of the meteorological masts Greater Gabbard (GG), Egmond aan Zee (EAZ), FINO1 and Horns Rev M2 (M2) are shown. The eight new offshore wind farm areas in Denmark are indicated: Horns Rev III (HR III), North Sea South (NSS), North Sea North (NSN), Sæby, Sejerøbugten (Sejerø), Smålandsfarvandet (Sf), Kriegers Flak (KF) and Bornholm.

Atmospheric stability is measured by means of the Obukhov length and it is estimated from the bulk Richardson number as in Grachev and Fairall (1996). The bulk Richardson number is computed using the air-sea potential temperature difference, humidity and pressure observations (see Peña, Gryning, & Hasager, 2008 for details). The Obukhov length is assumed to be constant within the surface layer. The estimation of the Obukhov length is performed in this study for the specific observed height (higher than 10 m but it depends on the site observational levels) and is assumed to be valid for 10 m height. Thus the stability correction to the logarithmic wind profile can be estimated at the specific height and at 10 m from the formulations in Peña et al. (2012). Thereafter the friction velocity is calculated from the diabatic wind profile as in Peña et al. (2008) assuming Charnock's relation for the roughness of the sea (see Peña & Gryning, 2008). This is the method of adding stability correction to the logarithmic wind profile. When no stability information is available, the friction velocity is estimated from the logarithmic wind profile directly.

It is important to notice that stability correction was only possible at Egmond aan Zee and M2 thus the 10 m wind speed is estimated from the diabatic wind profiles whereas for Greater Gabbard and FINO1 the logarithmic wind profile is used.

2.4. Wind resource statistics methodology

Wind resource estimation is usually based on meteorological observations collected as time-series of hourly or 10-minute recorded observations (usually from 10-min averages) over a minimum of one year, but preferable from several years as this reduces the uncertainty of the estimation. The data can be treated in the Wind Atlas Analysis and Application program (WAsP) (Mortensen et al., 2000) which uses the wind atlas methodology. This is the de facto standard method in wind resource assessment. The usual procedure is to divide the data into twelve 30° wind direction sectors and determine the Weibull scale and shape parameters in each sector (Troen & Petersen, 1989).

The number of satellite ocean wind observations in a single direction bin may be very small due to the observational frequency from space (e.g. Hasager et al., 2006). Thus alternatives to WAsP are developed (Nielsen, Astrup, Hasager, Barthelmie, & Pryor, 2004). The program is called Satellite-WAsP (S-WAsP) (Hasager et al., 2008). The second moment fitting for the Weibull scale (A) and shape (k) parameters (Barthelmie & Pryor, 2003; Pryor, Nielsen, Barthelmie, & Mann, 2004)

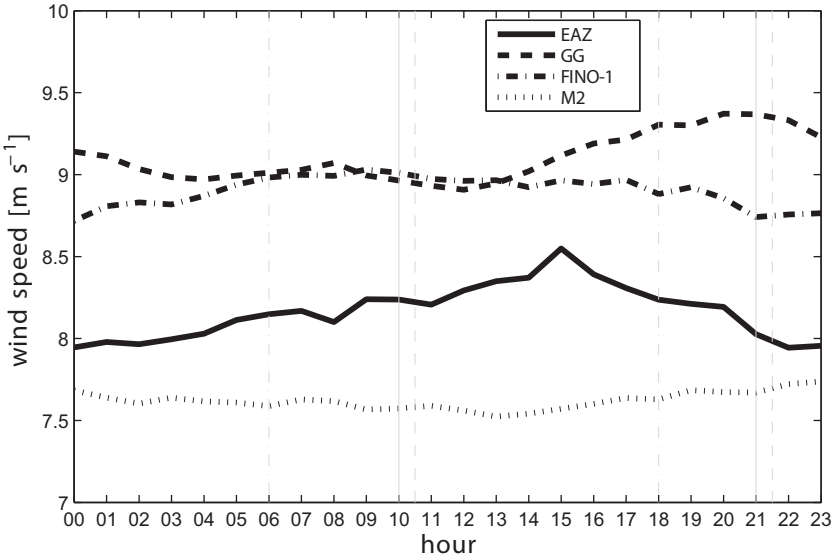

Fig. 5. Average diurnal wind speed (m s^{-1}) observed at four meteorological masts in the North Sea: Egmond aan Zee (EAZ) at 21 m using 72,602 10 minute values from February 2006 to November 2008, FINO1 at 33 m using 72,640 10 minute values from January 2004 to December 2006, Greater Gabbard (GG) at 42.5 m using 150,426 10 minute values from January 2006 to December 2009 and Horns Rev M2 (M2) at 15 m using 2,144,370 10 minute values from January 2003 to December 2006. The approximate local overpass times of QuikSCAT (06 and 18), ASCAT (10 and 21) and Envisat (10:30 and 21:30) are indicated.

can be used to fit a distribution to all data and estimate the two Weibull parameters. Thereafter the shape parameter can be assumed valid for all wind directions. Finally the binned wind speed data can be analysed and the scale parameter estimated for each wind directional bin. The available wind power density, E, is calculated from the two Weibull parameters using the gamma function Γ and the air density ρ (~1.245 g m^{-3} at 10 ° C at sea level) as

$$E = \frac{1}{2}\rho A^3 \Gamma\left(1+\frac{3}{k}\right). \quad (1)$$

More samples reduce the statistical uncertainty. The statistical uncertainty of using satellite observations for wind resource estimation (Barthelmie & Pryor, 2003; Pryor et al., 2004) shows that the mean wind speed and the Weibull scale parameter can be estimated reasonably well from around 70 samples for an uncertainty of ±10% at a confidence level of 90% whereas the energy density and Weibull shape parameter require around 2000 samples to obtain a similar uncertainty and confidence level. In case many samples are available the choice of Weibull fitting method is not critical (Barthelmie & Pryor, 2003; Pryor et al., 2004).

3. Comparison results

Comparison of scatterometer and SAR data to co-located meteorological observations is performed to assess sensor performance in the study area. For SAR the study involves several GMFs and selection of one of these for the synergetic analysis has been done (Section 3.1).

Linear regression analysis is performed. For QuikSCAT (v4) we find for FINO1 bias 0.09 m s^{-1} (Root Mean Square Error (RMSE) 1.15 m s^{-1}) based on 692 co-located samples and for Horns Rev M2 bias 0.16 m s^{-1} (RMSE 1.31 m s^{-1}) based on 1589 co-located samples. For Greater Gabbard 184 co-located samples give bias 1.64 m s^{-1} (RMSE 1.61 m s^{-1}) and for Egmond aan Zee bias 1.41 m s^{-1} (RMSE 1.22 m s^{-1}) based on 1267 co-located samples. We assume the positive bias of QuikSCAT at the near-coastal stations may be due to land effects in QuikSCAT. Karagali et al. (2014) reported similar results for QuikSCAT (v3). QuikSCAT (v4) comparison results to WindSat satellite winds show no bias and 0.9 m s^{-1} standard deviation (Ricciardulli & Wentz, 2011). For ASCAT too few co-located samples are available for similar analysis (see Table 4). An earlier study on ASCAT validation using triple collocation show that KNMI products have about 1.0 m s^{-1} wind vector precision and 1% accuracy (Vogelzang et al., 2011).

3.1. Comparison of in situ and SAR-derived wind speeds using three GMFs

The 10 m wind speeds from Horns Rev M2 and Egmond aan Zee are used to test the SAR-derived wind speeds from three GMFs. CMOD5 provides stability-dependent wind speed (Hersbach et al., 2007) whereas CMOD5N (CMOD5N, 2013) and CMOD-IFR2 provide equivalent neutral winds (Quilfen et al., 1998; Quilfen, pers.com.). Portabella and Stoffelen (2009) show that the difference between mean equivalent-neutral and stability-dependent wind speeds equals by good approximation 0.2 m s^{-1} for all wind speeds. At Horns Rev M2 using 150,310 10-minute samples from January 2003 to May 2007 show mean equivalent neutral wind only 0.07 m s^{-1} higher than mean stability-dependent wind (RMSE 0.36 m s^{-1}).

The wind data extrapolated to 10 m and averaged to hourly means collocated versus SAR-derived wind speeds from an area around 5 km by 5 km centred at the mast are compared. The observations from Egmond aan Zee and Horns Rev M2 versus CMOD-IFR2 are shown in Fig. 6. Table 3 shows the linear regression analysis results from Egmond aan Zee and Horns Rev M2 versus CMOD-IFR2, CMOD5 and CMOD5N.

The CMOD5, CMOD5N and CMOD-IFR2 statistical results are fairly comparable. The reason for the better agreement between SAR and meteorological mast winds at Horns Rev M2 may be because only a limited sector with wind farm influences the met data. A wind farm adjacent to the meteorological mast at Egmond aan Zee may cause more deviation from a logarithmic profile there. The measurements are collocated and only disturbances that affect one system but not the other cause discrepancy. In the subsequent analysis only CMOD-IFR2 results are presented. The choice of GMF is not easy but for CMOD-IFR2 the intercept is closer to zero and the slope closer to one. For FINO1 the linear

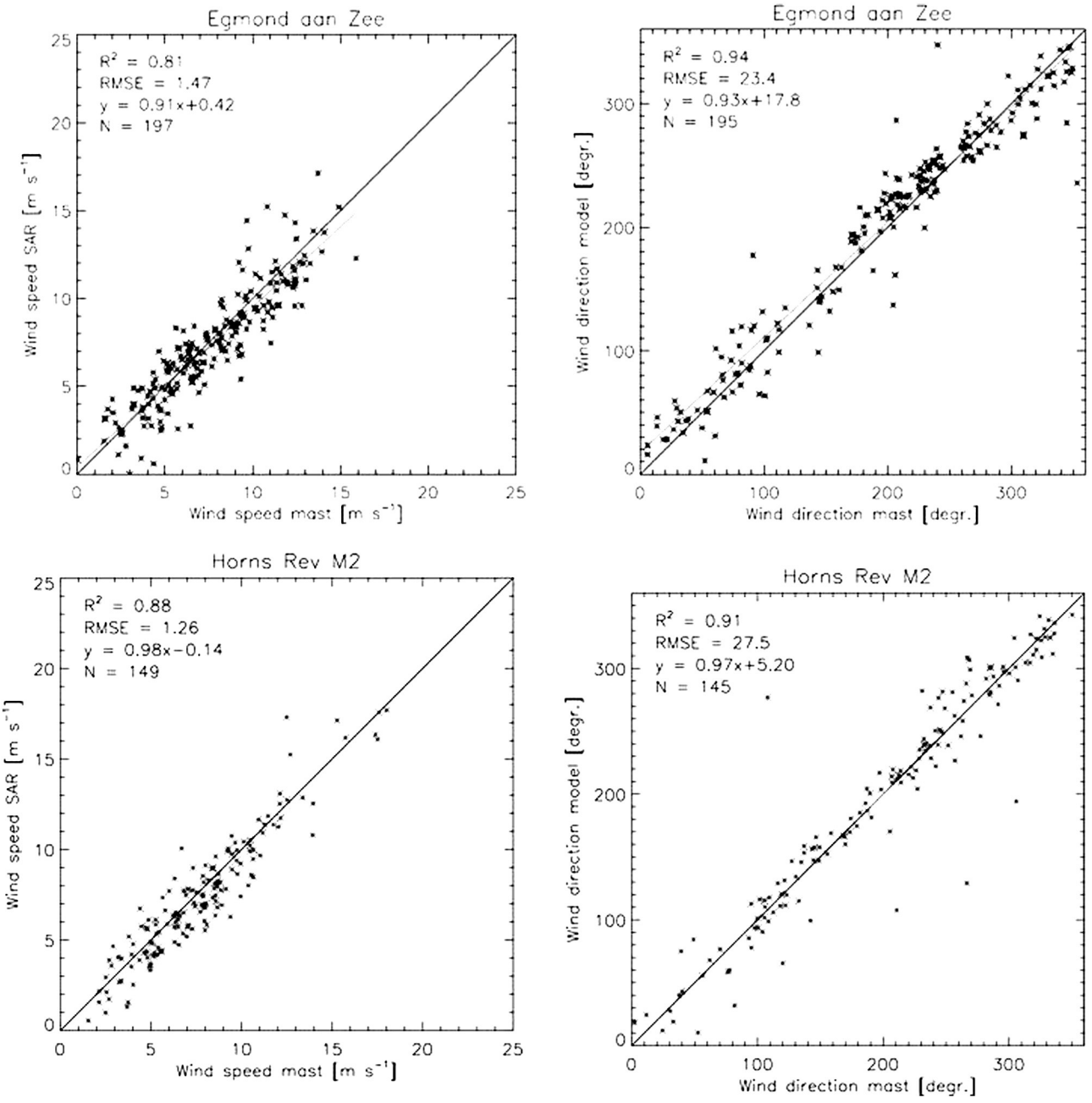

Fig. 6. Comparison of wind speed (left) and wind direction (right) of observations at the meteorological mast and SAR-based wind maps using CMOD-IFR2 for winds in the range 0–25 m s^{-1} for Egmond aan Zee (above) and Horns Rev M2 (below) for equivalent neutral winds at 10 m. The correlation coefficient squared (R^2), root mean square difference (RMSE), linear regression slope and intercept, and the number of samples (N) are included. Few samples of wind direction are omitted near 0°/360°.

correlation statistics using CMOD-IFR2 and 500 collocated meteorological mast samples is R^2 0.73 and RMSE 1.90 m s^{-1}. For Greater Gabbard R^2 is 0.69 and RMSE is 1.85 m s^{-1} based on 29 samples. The lower R^2 and higher RMSE at the two latter sites compared to Egmond aan Zee and Horns Rev M2 are assumed to be due to lack of stability data for the vertical extrapolation of the wind profile.

Table 3
Linear regression analysis results comparing meteorological mast winds extrapolated to 10 m at Egmond aan Zee and Horns Rev M2 and with SAR-derived wind speed from CMOD5, CMOD5N and CMOD-IFR2 for the wind speed range 0–25 m/s for stability-dependent winds at 10 m (U10) and equivalent neutral winds at 10 m (U10N).

	Horns Rev M2			Egmond aan Zee		
	CMOD5 U10	CMOD5 U10N	CMOD-IFR2 U10N	CMOD5 U10	CMOD5N U10N	CMOD-IFR2 U10N
R^2 (−)	0.85	0.86	0.87	0.78	0.79	0.81
RMSE (m s^{-1})	1.27	1.34	1.28	1.50	1.65	1.47
Slope (−)	0.93	0.92	0.97	0.85	0.84	0.91
Intercept (m s^{-1})	0.41	1.22	−0.08	1.17	1.93	0.42
N (−)	146	146	146	197	197	197

Table 4
Mean wind speed observed from all available satellite data and from co-located data at four meteorological masts. The number of samples (N) is indicated. The mean wind speed (U) from satellite and meteorological mast and the difference in percentage ((U_satellite minus U_meteorological mast) / U_meteorological mast * 00%).

	EAZ		FINO1		GG		M2	
	U sat all ($m\ s^{-1}$) (N)	U sat/ U met ($m\ s^{-1}$) (N)	U sat all ($m\ s^{-1}$) (N)	U sat/ U met ($m\ s^{-1}$) (N)	U sat all ($m\ s^{-1}$) (N)	U sat/ U met ($m\ s^{-1}$) (N)	U sat all ($m\ s^{-1}$) (N)	U sat/ U met ($m\ s^{-1}$) (N)
SAR	7.13 (662)	7.34/7.61 (197)	7.78 (641)	7.83/8.08 (500)	7.67 (815)	10.60/11.06 (29)	7.72 (924)	7.15/7.82 (468)
ASCAT	9.56 (242)	9.24/7.31 (157)	7.90 (519)	(0)	8.29 (530)	10.28/10.12 (27)	7.83 (440)	(0)
QSCAT	8.41 (5679)	8.44/7.63 (1267)	8.04 (6564)	8.19/8.16 (694)	8.26 (6565)	10.64/10.17 (184)	8.00 (5593)	7.58/7.54 (1589)
SUM	8.33 (6562)	8.39/7.60 (1621)	8.01 (7898)	8.04/8.13 (1194)	8.21 (7757)	10.50/10.27 (240)	7.95 (6957)	7.48/7.60 (2057)
Diff. (%)		10%		−1%		3%		−2%

3.2. Comparison of combined satellite data set

The previous section shows Envisat ASAR and QuikSCAT data are comparable and have same order of magnitude for the linear regression results when compared to the meteorological data in the study area. This forms the basis for synergetic use. The mean wind speed observed from each satellite sensor collocated at the four masts is listed in Table 4. In addition the number of available collocated samples, all satellite samples and mean wind speed from all satellite data are presented. The deviation in mean wind speed between co-located meteorological data and satellite data using the combined data set is small for FINO1 (−1%), Greater Gabbard (3%) and Horns Rev M2 (−2%) but high for Egmond aan Zee (10%). The latter most likely is due the mast being near the coast and scatterometer winds are over-predicted because the nearest grid cells are located further offshore than the mast for ASCAT and QuikSCAT. Collocated SAR wind speeds compare well at Egmond aan Zee. At Greater Gabbard only few co-located samples are available (in total 240) and the full satellite data set (7757 samples) show much lower wind speed. At FINO1 and M2 the mean wind speed differences of co-located data are less than 1% for QuikSCAT but for SAR under-predicted around 3% and 8%, respectively. The results on mean wind speed from all available satellite data combined is discussed further in Section 3.4 and Table 5. The linear regression results using all co-located data combined from Envisat ASAR, ASCAT and QuikSCAT for the wind speed range 0–25 $m\ s^{-1}$ have R^2 (RMSE) for Egmond aan Zee 0.82 (1.41 $m\ s^{-1}$), FINO1 0.82 (1.53 $m\ s^{-1}$), Greater Gabbard 0.79 (1.63 $m\ s^{-1}$) and Horns Rev M2 0.85 (1.34 $m\ s^{-1}$). The results are heavily influenced by QuikSCAT that contributes most samples at all masts. Thus the results also resemble results in Karagali et al., 2014.

3.3. Wind resource statistics for SAR, ASCAT and QuikSCAT

The wind resource statistics for the Northern European Seas are presented as individual maps for each satellite sensor as well as combined from all three. Fig. 7 shows the number of overlapping samples, the mean wind speed and energy density from SAR at 2 km, ASCAT at 12.5 km and QuikSCAT at 25 km.

The number of samples from QuikSCAT is much higher than from the other sensors. In the Baltic Sea the sea ice mask in QuikSCAT is far too conservative compared to actual sea ice. It results in relatively few samples. From ASCAT we mainly have data from the North Sea. In the Baltic Sea the number of ASCAT samples is below 100 and subsequently this area is omitted from wind resource calculation. From Envisat both the Baltic Sea and North Sea are covered well. The number of overlapping SAR scenes ranges from around 450 in parts of the Irish Sea to more than 1400 in parts of the North and Baltic Seas. Only in the northwestern part of the study area (Atlantic Ocean) the number of observations is rather low, i.e. less than 200 overlapping samples.

The three mean wind speed maps in Fig. 7 show similar wind speed pattern in the open seas. The main similarities are the pronounced lee effects east of the British Isles and higher winds north of Scotland extending eastwards to Norway. Along the Wadden Sea coast near the Netherlands and Germany the mean wind speed is lower than further north along the Danish west coast. In the central Baltic Sea the mean wind speed is higher than further north. The mean wind speed ranges from around 7 $m\ s^{-1}$ near many coastlines and in parts of the Baltic Sea up to around 10 $m\ s^{-1}$ in the northern part of the North Sea. Discrepancy in mean wind speed is found between SAR and scatterometer winds north of the UK with SAR seemingly over-estimating, most likely due to too few SAR samples, but it could also be due to physical phenomenon (sea surface temperature, ocean current, or other).

One of the obvious differences in the three maps is the higher spatial resolution in SAR that provides much clearer coastal wind speed gradients than ASCAT and QuikSCAT. Only SAR truly covers the near-shore coastal regions hence observe the lower winds. The offshore winds along most coastlines show a deep blue colour in the Envisat ASAR mean wind speed map, thus very fine scale wind patterns are visible. The deep blue colour corresponds to 6 $m\ s^{-1}$.

We also note some common artefacts in the satellite winds. For example, in between the Shetland Islands and Norway extensive oil exploration is going on. The associated structures at sea may cause corner reflections in radar backscatter data from SAR, ASCAT and QuikSCAT. These local structures are visible in the maps. Moreover, at low backscatter values also ships are visible, see, e.g., the enhanced winds near the Rotterdam harbour anchorage due to ships in ASCAT. Ships move and cannot be easily treated as land pixels. In scatterometer wind processing (ASCAT and QuikSCAT) geophysical anomalies are detected in the wind inversion step by the inversion residual or maximum likelihood estimation (Portabella & Stoffelen, 2002). This is how rain, fronts and other areas with rather extreme wind variability are flagged. The ASCAT screening is effective in screening out structures at sea, which are most dominant at low winds. Rejecting mainly low winds obviously causes a wind speed bias with respect to the true mean wind, i.e., a so-

Table 5
Number of years for satellite data combined (Sat) from 1999 to 2012 (14 years) for FINO1, Horns Rev M2, Egmond aan Zee (EAZ),and Greater Gabbard (GG), mean wind speed (U) and energy density (E). For FINO1 and Horns Rev M2 results from Badger et al., 2010 (B.2010) and Karagali et al., 2014 (K.2014) are listed based on meteorological mast data extrapolated to 10 m.

	FINO1			Horns Rev M2			EAZ	GG
	Sat	B.2010	K.2014	Sat	B.2010	K.2014	Sat	Sat
Years	14 U10N	5 U10	4 U10N	14 U10N	4 U10	3 U10N	14 U10N	14 U10N
U ($m\ s^{-1}$)	8.01	8.12	8.35	7.95	7.78	7.76	8.33	8.21
E ($W\ m^{-2}$)	549	561	578	535	499	451	574	538
N	7898	192,479	50,349	6957	200,050	137,717	6562	7757

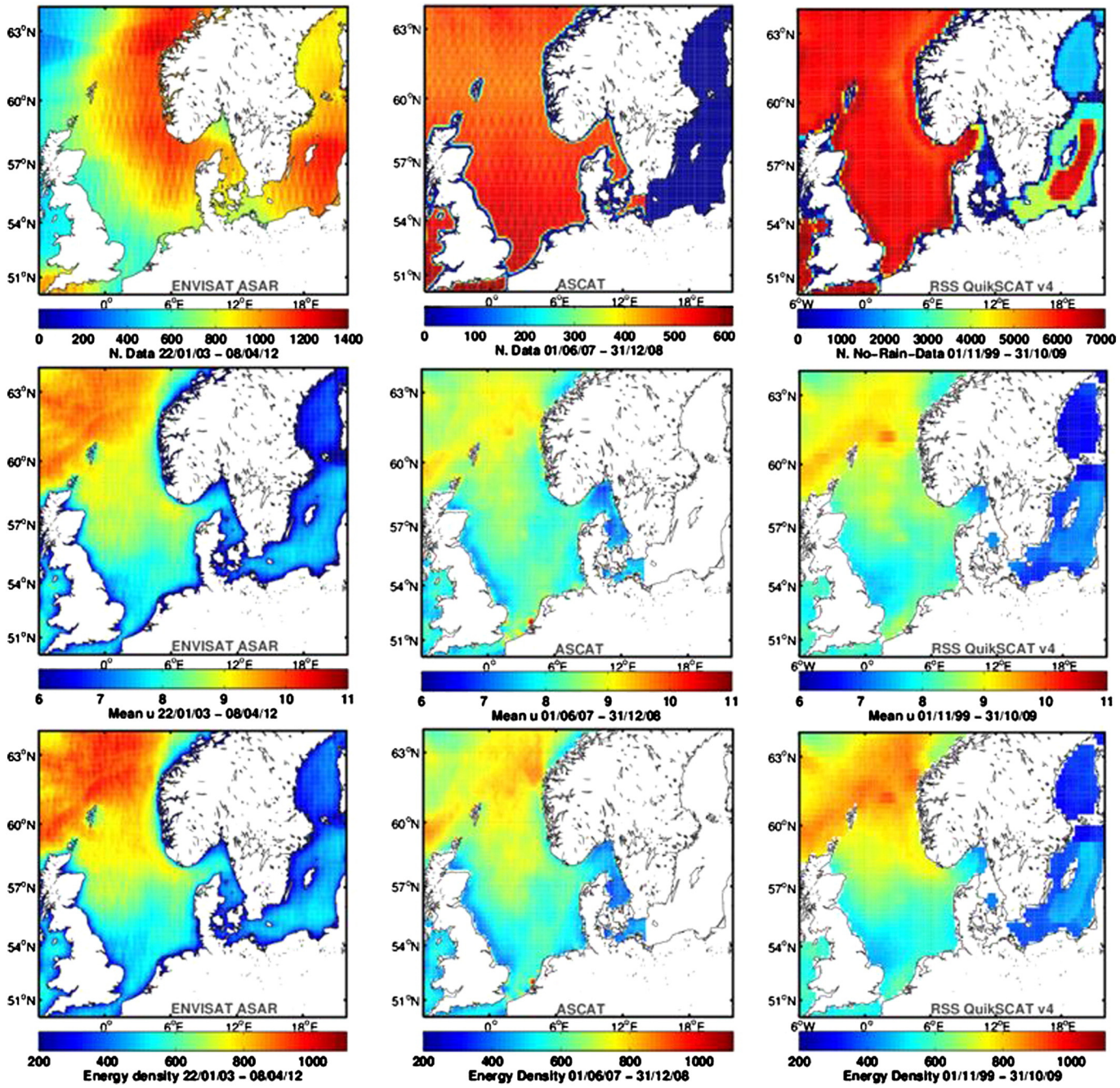

Fig. 7. Number of overlapping samples (top panel), mean wind speed (middle panel) and energy density (lower panel) from Envisat ASAR at 2 km from 2003 to 2012, ASCAT at 12.5 km from 2007 to 2008 and QuikSCAT at 25 km from 1999 to 2009 are shown for the Northern European Seas. Please note the colour scale for the number of overlapping samples varies for the three satellites. (For interpretation of the references to colour in this figure legend, the reader is referred to the web version of this article.)

called sampling bias. QuikSCAT data used in this study are all flagged as rain-free, but despite this, sampling error due to rain may still occur and the screening may reject unstable winds (false alarms). In SAR removal of small hard targets was applied before wind inversion so the problem is expected to be minor for the wind speed retrieval in SAR. Also in SAR hard targets are most easily removed at low winds, but due to the small footprint relatively fewer samples may be affected by the quality control.

The energy density maps from SAR, ASCAT and QuikSCAT (Fig. 7 lower panels) show the same similarities as described for the mean wind speed maps. The energy density ranges from 200 W m^{-2} near some coastlines to more than 1000 W m^{-2} in parts of the Atlantic Sea.

The number of samples needed to estimate the energy density is much higher than to estimate the mean wind speed (Barthelmie & Pryor, 2003; Pryor et al., 2004). An example of the statistical uncertainty on energy density is presented. When using only the wind speed maps observed by SAR and following the equations from the appendix in Pryor et al. (2004), the map of uncertainty on energy density is calculated and shown in Fig. 8. In this it is assumed that each SAR-based wind map is accurate and that the influence of time sampling is insignificant to the estimates. In other words, we assume the diurnal wind pattern to be described accurately using morning and evening observations only. Thus the map shows the statistical uncertainty as a function of number of samples. It is noticed that for most of the study area the uncertainty is

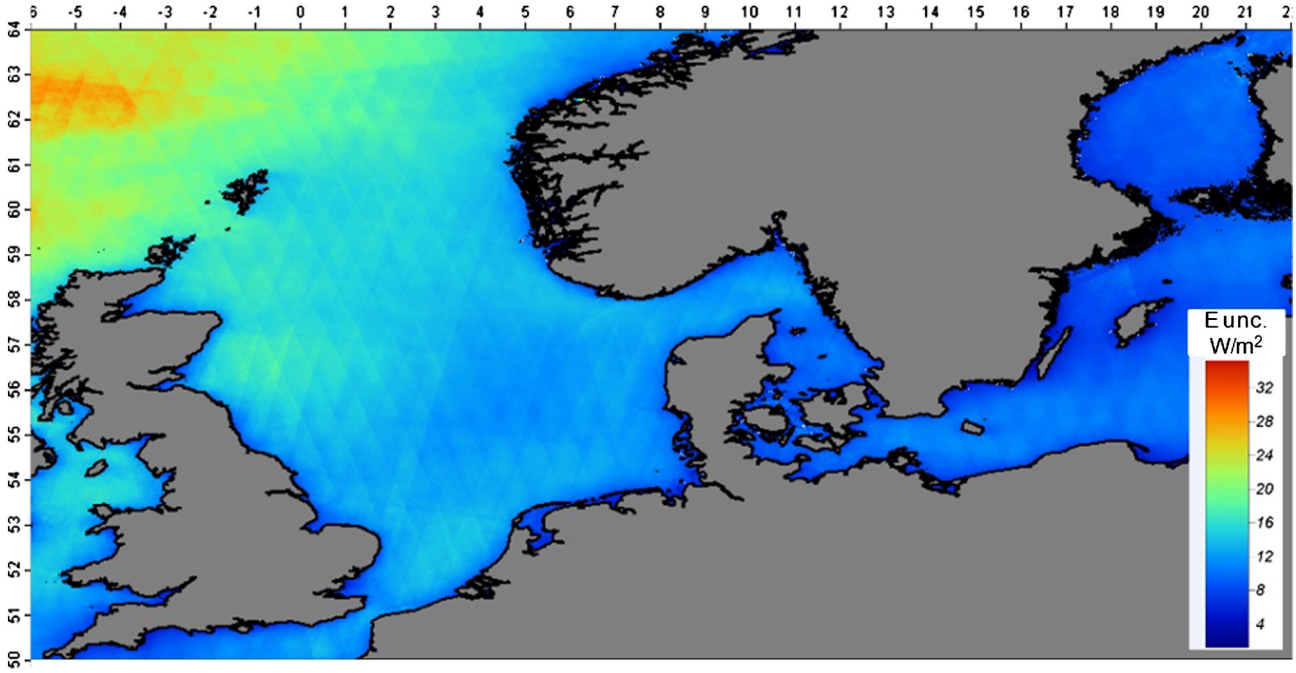

Fig. 8. Map of the uncertainty on energy density (E unc.) using Envisat ASAR wind maps covering the Northern European Seas.

below 15 W m^{-2} but in the north-western part (Atlantic Ocean) the number of samples is rather low. This causes statistical uncertainty on energy density around 20 to 30 W m^{-2}.

3.4. Wind resource statistics from synergetic satellite data

Synergetic use of wind maps from SAR, ASCAT and QuikSCAT for wind resource estimation has two obvious advantages: i) the number of samples increase thus the statistical uncertainty is reduced; ii) the observations are taken during more overpass times thus at sites with pronounced diurnal wind variations a better representation is expected.

The synergetic maps combining SAR, ASCAT, and QuikSCAT are shown in Fig. 9. The combination is done collecting samples from each data source using a regular grid defined. Only grid cells with their centre close to the regular grid are used. For each 2 km grid cell statistics of mean wind speed, Weibull fitting for scale and shape parameters using maximum likelihood estimator and energy density Eq. (1) is calculated. The number of samples is high, thus the choice of Weibull fitting is not critical.

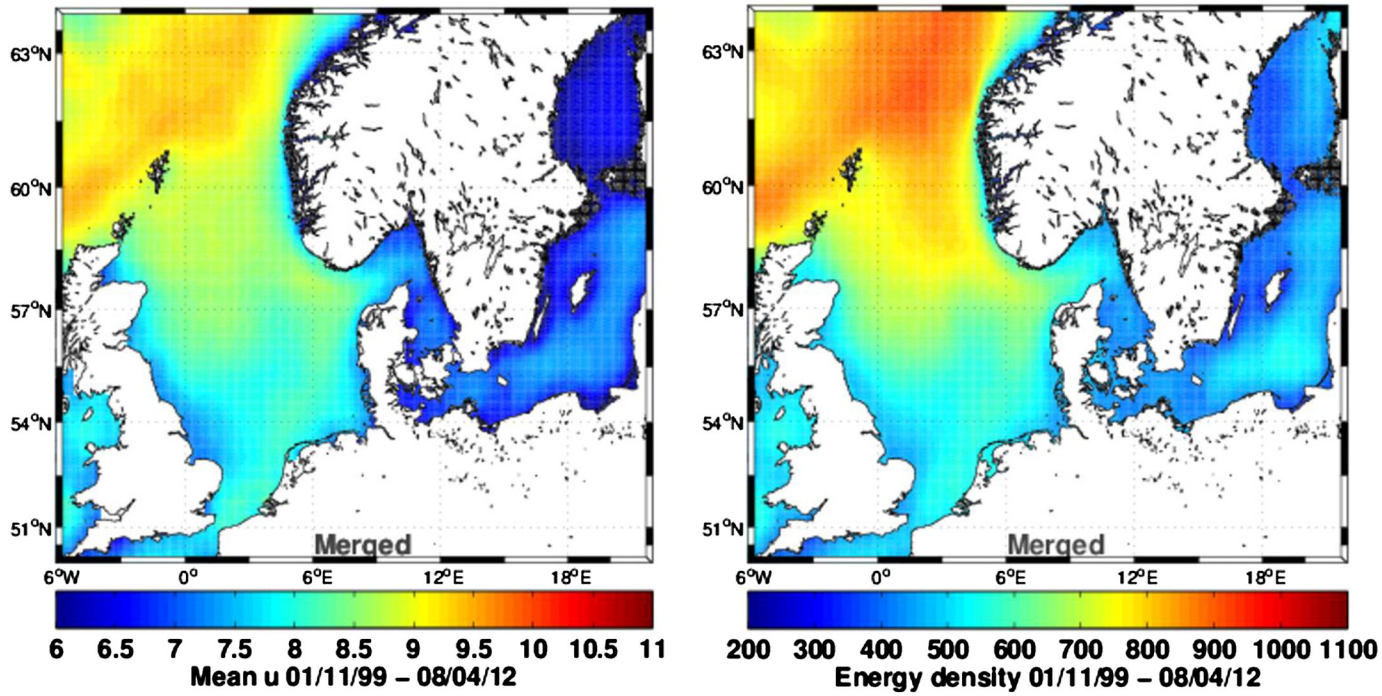

Fig. 9. Synergetic use of Envisat ASAR (2002 to 2012), ASCAT (2007 to 2008) and QuikSCAT (1999 to 2009) for the Northern European Seas: mean wind speed m s^{-1} (left) and energy density W m^{-2} (right).

The maps of mean wind speed and energy density show all dominant spatial patterns to be well represented comparing to the results in Fig. 7. Near the coastlines the SAR-based details contribute to map the spatial gradients on ocean winds better than scatterometer data alone.

The number of satellite samples combining SAR, ASCAT and QuiksCAT is high, from more than 6500 to nearly 7900 at the four meteorological masts. The mean wind speed and energy density results are presented in Table 5. The results are based on data spanning 14 years from 1999 to 2012. The number of samples from each sensor is listed in Table 4.

Comparison to *collocated* samples (see Table 4) is based on relatively few samples when keeping in mind how many samples are needed for energy density estimation. Therefore, as an alternative, the results on mean wind speed and energy density from the combined satellite data set are compared to *non-collocated* in situ wind statistics from (Badger et al., 2010) and (Karagali et al., 2014). Both have calculated mean wind speed and energy density at FINO1 and Horns Rev M2 but Badger et al. (2010) have reported statistics from the stability-dependent wind speed (for comparison to U10) whereas Karagali et al. (2014) reported statistics from equivalent neutral wind speed (for comparison to U10N). Badger et al., 2010 used a 1-year longer data set at both masts. For the vertical extrapolation different approaches are selected and these resulted in very different numbers of observations with Karagali et al. (2014) using a conservative approach resulting in far fewer samples. Selected results from Badger et al. (2010) and Karagali et al. (2014) are listed in Table 5.

It is noted that at FINO1 the difference in mean wind speed for U10N and U10 is around 0.23 m s^{-1} and it compares well to the result of 0.2 m s^{-1} (Portabella & Stoffelen, 2009). At M2 the difference between mean wind speed U10N and U10 is slightly negative. However, the results from the present study based on 150,310 samples show U10N to be on average 0.07 m s^{-1} larger than U10. It is concluded that the slightly negative value between U10N and U10 from Badger et al. (2010) and Karagali et al. (2014) must be due to different sampling and meteorological data processing.

The above variations in sampling and meteorological data processing add to overall difficulties in validation of the synergetic wind resource statistics to non-collocated statistics. The synergetic satellite data are U10N thus it is expected these compare the best to results from Karagali et al. (2014).

At Horns Rev M2 the mean wind speed from combined satellite data is around 3% higher than meteorological data. For energy density the satellite data gives 19% higher than Karagali et al. (2014) but only 7% higher than Badger et al. (2010). At FINO1 the mean satellite wind speed is around 4% lower and energy density is 5% lower between satellite data and results in Karagali et al. (2014). Comparison results between mean satellite wind speed and energy density from combined satellite data and results in Badger et al. (2010) show 0 and 2% differences, respectively.

At Egmond aan Zee the combined satellite data set gives mean wind speed 8.33 m s^{-1} and energy density 574 W m^{-2} and at Greater Gabbard mean wind speed 8.21 m s^{-1} and energy density 538 W m^{-2}. In case the results at Egmond aan Zee in Table 4 with 10% higher mean wind speed from satellite data than collocated meteorological data also occur in the combined satellite data set, the energy density is most likely overestimated. Comparison results are not available so no further assessment on mean wind speed and energy is possible for Egmond aan Zee and Greater Gabbard.

The combined satellite data set has been used to calculate wind roses at the four sites. For comparison meteorological mast data at the lowest level are used except at FINO1 at 60 m. The results are presented in Fig. 10. The results are based on observations from Egmond aan Zee 02/2006 to 11/2008 (72,602 10 minute samples), FINO1 01/2004 to 12/2006 (72,640 10 minute samples), Greater Gabbard 01/2006 to 12/2009 (150,426 10 minute samples) and Horns Rev M2 01/2003 to 12/2006 (144,370 10 minute samples). The wind roses show good correspondence.

3.5. Wind resource statistics for the new Danish wind farm areas

One of the advantages of SAR-based wind resource mapping is the high spatial resolution. Most grid connected offshore wind farms are located within 25 km from the coastline. Thus SAR-based wind resource maps have particular relevance. The near-shore coastal zone can be observed and, in those, relatively high spatial gradients in horizontal wind speed are expected. As an example the new Danish wind farm areas are investigated.

There are eight new areas in planning for offshore wind farms in Denmark (see Fig. 4). The two larger areas are located relatively far offshore. These are Kriegers Flak of 250 km^2 in the Baltic Sea and Horns Rev 3 of 200 km^2 in the North Sea. Kriegers Flak is located 15 km from the nearest coast of the island Møn. Horns Rev 3 is located 10 to 30 km from the nearest coast of Jutland. According to DEA (DEA, 2013) the mean wind speed at Kriegers Flak is 9.5 m s^{-1} and at Horns Rev 3 is 9.8 m s^{-1} (the height is not given). The six smaller near-shore areas are located at least 4 km offshore from the nearest coastline. The mean wind speeds are not given for the smaller areas. It is found that the number of overlapping Envisat ASAR wind speed maps in the eight areas is around 900 (ranging from 801 to 980).

The mean energy density as well as the minimum and maximum energy density within each area are calculated and shown in Fig. 11. The graph shows the sites ranked from lower to higher mean energy density. The mean energy density at Sejerøbugten is 347 W m^{-2}. The mean energy density at Horns Rev 3 is 514 W m^{-2}. In addition, the area of each site is indicated in Fig. 11. It is noticeable that the maximum range in wind speed is not related to the size of the area. Kriegers Flak is the largest but has minimum variation in energy density of only 20 W m^{-2} (ranging from 417 to 437 W m^{-2}). In contrast, some smaller areas have a much wider range in energy density, e.g. Smålandsfarvandet has a range of 76 W m^{-2} (from 325 to 401 W m^{-2}). It is observed that much higher spatial variability in winds is found in the near-shore coastal areas than at the sites further offshore.

The statistical uncertainty on energy density vary from 8 W m^{-2} at Sæby and Sejerøbugten, to 9 W m^{-2} at Smålandsfarvandet, 10 W m^{-2} at Kriegers Flak, North Sea North and North Sea South and up to 11 W m^{-2} at Horns Rev 3. The statistical uncertainty on mean wind speed varies around 0.6 to 0.7 m s^{-1} at the sites. This is for an uncertainty of $\pm$10% at a confidence level of 90%. This is again assuming the SAR-based winds to be accurate and representative of the diurnal wind variation. The mean wind speeds observed from Envisat ASAR at 10 m are at Sejerøbugten 6.8 m s^{-1}, Sæby 6.6 m s^{-1}, Smålandsfarvandet 6.6 m s^{-1}, Kriegers Flak 7.3 m s^{-1}, Bornholmd 7.3 m s^{-1}, North Sea (north) and North Sea (south) 7.6 m s^{-1} and Horns Rev 3 7.8 m s^{-1}.

4. Discussion

Offshore wind resource estimation has a number of challenges. The general method applied to obtain an offshore wind atlas is through mesoscale modelling (Berge, Byrkjedal, Ydersbond, & Kindler, 2009). In mesoscale modelling numerous choices have to be done such as selection of re-analysis data input, planetary boundary layer scheme, sea surface temperature map among others (Hahmann et al., accepted for publication). The accuracy of model results is not fully clear mainly due to lack of offshore observations for validation. Increasing numbers of satellite observations are available for weather model validation. For scatterometer winds good error models exists. SARs are less well calibrated but potentially useful near the coast (after validation).

In the present study the number of collocated samples is limited. At all available meteorological masts the observations are from heights above 10 m, thus vertical extrapolation is necessary. It is optimal to use the diabatic profile but accurate additional meteorological data are

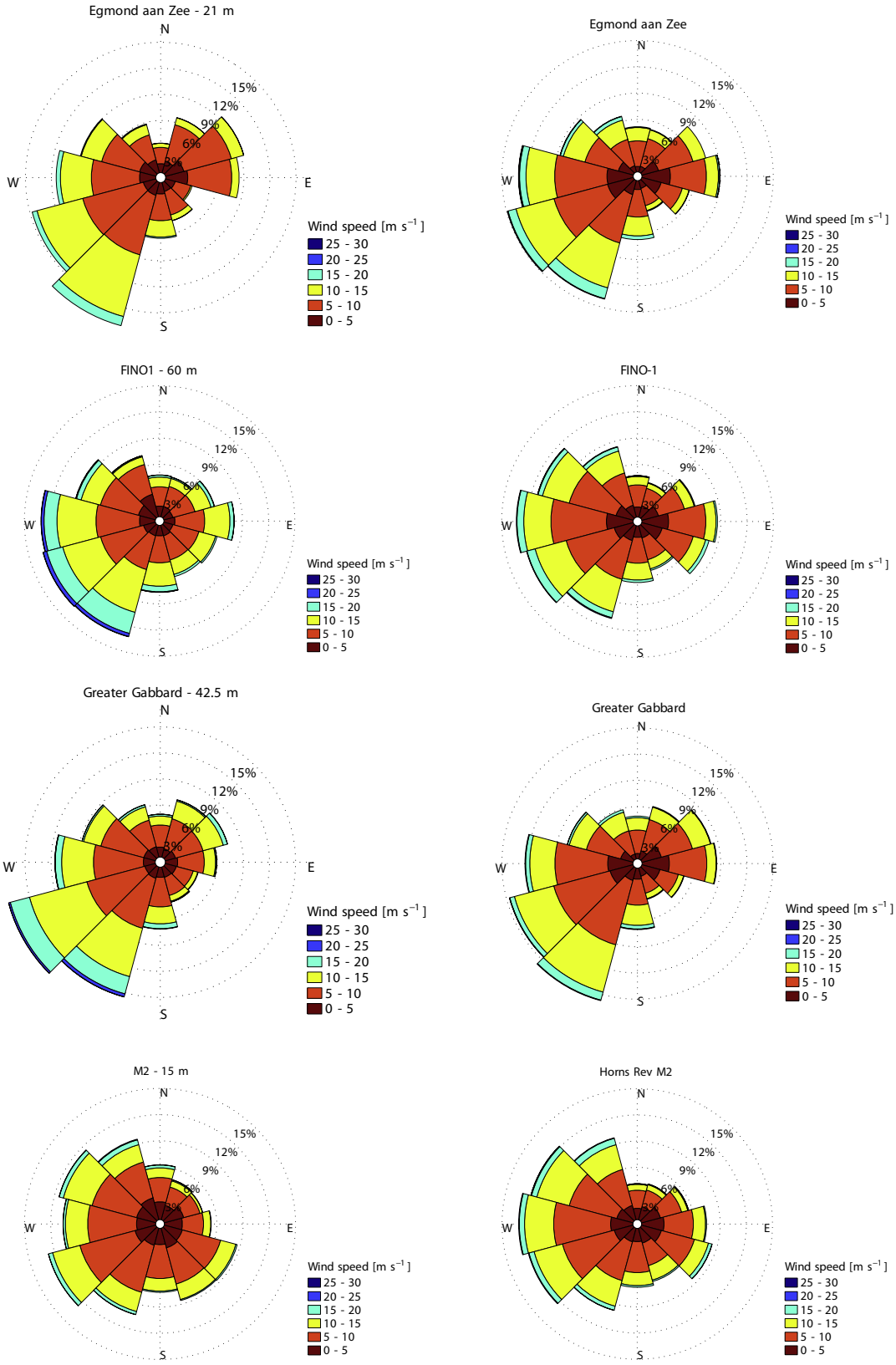

Fig. 10. Wind roses from Egmond aan Zee (02/2006 to 11/2008 (72,602 10 minute samples)) at 21 m, FINO1 (01/2004 to 12/2006 (72,640 10 minute samples)) at 60 m, Greater Gabbard (01/2006 to 12/2009 (150,426 10 minute samples)) at 42.5 m and Horns Rev M2 (01/2003 to 12/2006 (144,370 10 minute samples)) at 15 m observed at meteorological masts (left panels) and from three satellites combined (Envisat ASAR, ASCAT and QSCAT) (right panels).

not always available. CMOD-IFR2 was selected for SAR processing of the full archive of Envisat ASAR scenes but this choice was not easily done from the presented analysis. It is clear that the linear correlation statistics are better at meteorological masts for which the adiabatic profile is used. However, near all four meteorological masts wind turbines are located in the vicinity. This has two drawbacks. One is the observed

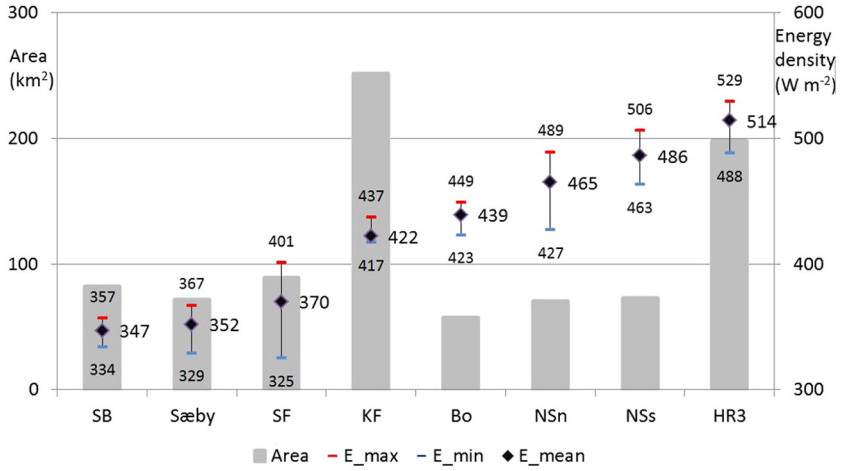

Fig. 11. Areal extend (km^2) of the eight new offshore wind farm areas in Denmark (1st y-axis) and energy density maximum (max), minimum (min) and mean (with values) ($W\,m^{-2}$) (2nd y-axis) at 10 m based on Envisat ASAR for locations Sejerøbugten (SB), Sæby, Smålandsfarvandet (SF), Kriegers Flak (KF), Bornholm (Bo), North Sea north (NSn), North Sea south (NSs) and Horns Rev 3 (HR3).

wind may not be representative of the free stream undisturbed flow due to wind farm wake effects that decelerate the flow; the other is that the wind turbines are hard targets and can act as corner reflectors and give very high return signals which may result in too high winds observed from the satellites.

The comparison of collocated samples for SAR provide results of similar quality as previous studies (Christiansen et al., 2006; Hasager et al., 2011) whereas the combined data set of collocated samples where QuikSCAT provide the majority are similar to results in Karagali et al., 2014 even though QuikSCAT v3 was used in the previous study and QuikSCAT v4 in the present. QuikSCAT samples represent by far the largest contribution to the synergy satellite data set, more than 75% at the four meteorological masts. Thus QuikSCAT dominates the results in the open ocean whereas SAR dominates in coastal regions. The meteorological mast observations are assumed to have around 0.2 $m\,s^{-1}$ accuracy for the sensor. Flow distortion from mast, booms, etc. should be accounted for. The linear regression is performed with the x-values assumed free of error in the present study. The distance to the nearest coastline is 15 km at Egmond aan Zee and 17 km at Horns Rev M2. For ASCAT and QuikSCAT this is near the limit of observation capability. Due to the relatively steep wind gradient near the coast and that the collocation procedure may result in an average distance of the scatterometer wind vector cells further away from the coast than the meteorological masts, biases may occur in their speed differences. Other factors that could increase satellite winds near the coasts are land and corner reflections.

The present study aims to progress beyond the accuracy of each individual sensor and GMF (even though the topic is important). The hypothesis is that additional usage of SAR for offshore wind resource estimation will increase the accuracy of offshore wind resource estimates compared to using scatterometer data only. For the coastal regions where only SAR is available this is obviously true. The wind resource statistics are dependent upon the number of samples. The observing times between ASAR and QuikSCAT differ by around three hours and for sites with diurnal wind variation there should be advantages combining data from several sensors. Based on the comparison with meteorological mast data we cannot conclude that the synergetic use of satellite products reduces the uncertainty. Reliable collocated samples are too few. The comparison results using collocated samples on the mean wind speed at four masts give few percent deviations around 1 to 3% for all masts but Egmond aan Zee with 10% overestimation by satellite. It could be due to proximity of a wind farm and the coastline and the wake influence to the meteorological mast data in a wide sector or the satellite samples collected (slightly) further offshore than the meteorological data. The mean wind speed from satellite based on 1621 collocated samples is 7.6 $m\,s^{-1}$ observed at the meteorological mast and 8.4 $m\,s^{-1}$ from satellite.

The maps of energy density from each individual data source show many similar large scale features in the open ocean. The combined map using Envisat ASAR, ASCAT and QuikSCAT in synergy provide a map with more spatial detail than the scatterometer maps alone. The statistical uncertainty using around 1000 SAR-based wind maps is less than 20 $W\,m^{-2}$ for $\pm$10% at a confidence level of 90%. In order to verify the results on energy density the number of collocated samples is too low. Comparison of combined satellite data to non-collocated in situ winds at Horns Rev M2 shows around 7–19% positive deviation and at FINO1 around 2–5% negative deviation on energy density dependent upon the selection and treatment of the in situ data and variation between stability-derived wind speed and equivalent neutral winds (ref. Badger et al., 2010; Karagali et al., 2014). Diurnal wind variation is negligible at the two sites. Besides sampling, at Horns Rev the overestimation from satellite may be due to reflection from the many wind turbines in the vicinity and for scatterometer maybe land effects or scatterometer sampling further offshore than the location of the mast. No clear conclusion can be drawn.

Comparison of wind roses using non-collocated in situ data observed at higher levels than 10 m with the combined satellite data set show good overall agreement. Diurnal wind speed variation at sea exist in some location and for those sampling winds from several satellites with different overpass times should improve the wind resource statistics but the data set has not been sufficient to demonstrate this. Possibly larger data sets including more satellite and in situ data will enable this in the future.

Model-based offshore wind climatology covering (parts of) the Northern European Seas include the European offshore wind resource (Petersen, 1992), the atlas of UK marine renewable energy resources (Atlas of UK Marine Renewable Energy Resources, 2008), the wind field map from ECMWF (EEA, 2009) and the South Baltic Sea wind atlas (Peña et al., 2011). Three maps show mean wind speed near hub-height above 8 $m\,s^{-1}$ in the North Sea (EEA, 2009; Peña et al., 2011; Troen & Petersen, 1989). Only the most recent (Peña et al., 2011) calculated with a resolution of 5 by 5 km show lower winds near the coastlines similar to the satellite-based results. The UK wind atlas shows energy density near hub-height calculated with a 12 by 12 km resolution and spatial patterns compare well to the satellite-based results.

The energy densities at the eight new Danish offshore areas for wind energy are examined from the SAR-based wind map. Two interesting

results emerged. Firstly, the mean energy densities vary considerably between the sites from 347 W m^{-2} at Sejerøbugten to 514 W m^{-2} at Horns Rev 3. Secondly, the variation in energy density within each area is strongly dependent upon proximity to the coastline. The variation in energy density is only 20 W m^{-2} at Kriegers Flak within a 250 km^2 large area far offshore whereas at Smålandsfarvandet the variation is 76 W m^{-2} within an area of 89 km^2. The statistical uncertainty is around 10 W m^{-2}, thus considerably less than the observed variation between wind farms and within each area. Smålandsfarvandet is characterized by several islands and a complex coastline. It is challenging to optimize the lay-out for a wind farm for an area with a spatially highly variable wind resource and to predict the expected annual energy production.

During the collocated comparison analysis, false values from in situ masts happen to be identified while comparing to satellite data. Further use of satellite data e.g. in near-real-time for quality control of winds observed at existing offshore meteorological masts and offshore lidars could be an advantage for further improving meteorological mast and lidar data availability. Soon after instrument failure such incident could be reported in case the more than 4000 daily satellite wind observation are used routinely. In wind resource estimation high data availability is needed for producing 'bankable' wind energy projects (e.g. Hasager et al., 2013). As is common practise in operational meteorology, meteorological mast observations may be monitored against numerical weather prediction (NWP) model fields, such that quality assurance of in situ data, satellite data and NWP modelling may be performed, as well as triple collocation analysis. The latter provides calibration and error analysis of all input data sources, including NWP model winds. Although NWP models may have their artefacts, NWP data do furthermore provide uniform sampling everywhere. Errors due to non-uniform data availability of satellite data are one of the important issues within this study but investigation of seasonal and decadal variations is outside scope of the present analysis but important for future investigation.

Wind resource estimation puts a high demand not only on the number of samples but also on the accuracy of each individual wind map. The hard targets at sea such as ships, wind turbines, oil and gas platforms and other structures give high backscatter. Removal of these effects is an important task for the future to increase the accuracy of satellite-based winds. Around 200 vessels can be active each day during the construction phase of a large wind farm. Furthermore shipping lanes and anchorage areas have a high number of ships. Another perspective for improved SAR-based wind mapping is automatic flagging of non-wind effects such as rain and ocean current. In near-coastal areas modified GMF could be developed as the available GMFs are valid for open-ocean. The wind and capillary waves may not be in full equilibrium, especially for offshore flow and short fetch.

With Sentinel-1A in orbit new ocean wind maps will become available. The future perspectives are to include observations from Sentinel-1, ASCAT B and other sensors, work on improving GMFs and removing noise from hard targets prior to applied synergy use for wind resource estimation. Last but not least refining methods for the extrapolation of 10 m winds to hub-height combining satellite and mesoscale model results for improved wind resource estimation in wind engineering (Badger, Peña, Hahmann, & Hasager, 2013) is in progress using climate stability information from mesoscale modelling (Peña & Hahmann, 2012).

5. Conclusion

Offshore wind resource estimation based on satellite remote sensing using active microwave instruments is investigated. Focus is on synergy use combining Envisat ASAR, ASCAT and QuikSCAT to increase the number of available samples such that energy density can be assessed with less statistical uncertainty. At the same time winds are observed at multiple times during the day and diurnal wind speed variation is better covered. The key results are energy density maps from three sensors which show much the same spatial variation in the open ocean. The combined result show mainly more spatial detail added from SAR. Based on collocated samples the difference in mean wind speed is −2%, −1% and 3% for Horns Rev Mast2, FINO1 and Greater Gabbard, respectively, but 10% at Egmond aan Zee. The latter result is most likely due to satellite scatterometer samples collected further offshore than the location of the meteorological mast. Comparing non-collocated samples at Horns Rev M2 shows overestimation from 7-19% and at FINO1 underestimation 2–5% on energy density but no clear conclusion can be drawn.

Significant coastal wind speed gradients are identified in SAR. In relationship to the eight new offshore wind farm areas in Denmark, the spatial variability based on SAR show mean energy density to range from 347 W m^{-2} in Sejerøbugten to 514 W m^{-2} at Horns Rev 3. The spatial variability in energy density is particularly high at some of the near-shore areas.

Acknowledgements

Funding for and collaboration within the FP7 NORSEWInD project TREN-FP7-219048 coordinated by Dr. Andy Oldroyd at Oldbaum Services is warmly acknowledged. Envisat data are provided by the European Space Agency. ASCAT data are provided by the Eumetsat OSI SAF and the Copernicus MyOcean services and QuikSCAT from Remote Sensing Systems. At DTU Wind Energy we are very thankful for collaboration with Frank Monaldo on the SAR processing. Meteorological observations are kindly made available for FINO1 from Federal Ministry for Environment (BMU), Horns Rev M2 from DONG energy and Vattenfall, Egmond aan Zee from NUON, and Greater Gabbard from SSE.

References

Badger, M., Badger, J., Nielsen, M., Hasager, C.B., & Peña, A. (2010). Wind class sampling of satellite SAR imagery for offshore wind resource mapping. *Journal of Applied Meteorology and Climatology*, *49*(12), 2474–2491, http://dx.doi.org/10.1175/2010JAMC2523.1.

Badger, M., Peña, A., Hahmann, A.N., & Hasager, C.B. (2013). Combining satellite winds and NWP modelling for wind resource mapping offshore. *ESA Living Planet Symposium, 9–13 September 2013, Edinburgh, United Kingdom.*

Barthelmie, R.J., Badger, J., Pryor, S.C., Hasager, C.B., Christiansen, M.B., & Jørgensen, B.H. (2007). Offshore coastal wind speed gradients: Issues for the design and development of large offshore wind farms. *Wind Engineering*, *31*(6), 369–382.

Barthelmie, R.J., & Pryor, S.C. (2003). Can satellite sampling of offshore wind speeds realistically represent wind speed distributions. *Journal of Applied Meteorology*, *42*(1), 83–94.

Beaucage, P., Bernier, M., Lafrance, G., & Choisnard, J. (2008). Regional mapping of the offshore wind resource: Towards a significant contribution from space-borne synthetic aperture radars. *IEEE Journal of Selected Topics in Applied Earth Observations and Remote Sensing (JSTARS)*, *1*(1), 48–56.

Berge, E., Byrkjedal, O., Ydersbond, Y., & Kindler, D. (2009). Modelling of offshore wind resources. Comparison of a meso-scale model and measurements from FINO1 and North Sea oil rigs. *Scientific Proceedings EWEC'09 Marseille, France*.

Brown, A.R., Beljaars, A.C.M., Hersbach, H., Hollingsworth, A., Miller, M., & Vasiljevic, D. (2005). Wind turning across the marine atmospheric boundary layer. *Quarterly Journal of the Royal Meteorological Society*, *131*, 1233–1250, http://dx.doi.org/10.1256/qj.04.163.

Capps, S.B., & Zender, C.S. (2010). Estimated global ocean wind power potential from QuikSCAT observations, accounting for turbine characteristics and siting. *Journal of Geophysical Research*, *115*, D09101, http://dx.doi.org/10.1029/2009JD012679.

Chang, R., Zhu, R., Badger, M., Hasager, C.B., Zhou, R., Ye, D., & Zhang, X. (2014w). *Applicability of SAR wind retrievals on offshore wind resources assessment in Hangzhou Bay*. Energies, special issue: Wind turbines (in review).

Choisnard, J., Lafrance, G., & Bernier, M. (2004). SAR-satellite for offshore and coastal wind resource analysis, with examples from St. Lawrence Gulf, Canada. *Wind Engineering*, *28*, 367–382.

Christiansen, M.B., Koch, W., Horstmann, J., Hasager, C.B., & Nielsen, M. (2006). Wind resource assessment from C-band SAR. *Remote Sensing of Environment*, *105*, 68–81.

Dagestad, K. -F., Horstmann, J., Mouche, A., Perrie, W., Shen, H., Zhang, B., et al. (2013). Wind retrieval from synthetic aperture radar — An overview. *Proceedings of SEASAR 2012, 4th SAR Oceanography Workshop (SEASAR 2012). Tromsø, Norway, 18–22 June 2013, ESA SP709* (pp. 22).

Ebuchi, N. (2013). Intercomparison of four ocean vector wind products from OceanSat-2 scatterometer. *International Ocean Vector Wind Science Team, Kona, Hawaii, 6–8 May 2013* (http://www.coaps.fsu.edu/scatterometry/meeting/docs/2013/First%20Results/Ebuchi_IOVWST2013.pdf).

EEA (2009a). Europe's onshore and offshore wind energy potential. An assessment of environmental and economic constrains. *EEA Technical Report No 6/2009* (pp. 90).
Fichtner (2012). Cost reduction potentials of offshore wind power in Germany. http://www.offshore-stiftung.com/60005/Uploaded/SOW_Download%7CEN_ShortVersion_CostReductionPotentialsofOffshoreWindPower.pdf
Furevik, B., Johannessen, O., & Sandvik, A.D. (2002). SAR-retrieved wind in polar regions — Comparison with in situ data and atmospheric model output. *IEEE Transactions on Geoscience and Remote Sensing, 40*, 1720–1732.
Furevik, B.R., Sempreviva, A.M., Cavaleri, L., Lefèvre, J. -M., & Transerici, C. (2011). Eight years of wind measurements from scatterometer for wind resource mapping in the Mediterranean Sea. *Wind Energy*, *14*(3), 355–372, http://dx.doi.org/10.1002/we.425.
Gerling, T.W. (1986). Structure of the surface wind field from the SEASAT SAR. *Journal of Geophysical Research*, *91*, 2308–2320.
Grachev, A.A., & Fairall, C.W. (1996). Dependence of the Monin–Obukhov stability parameter on the bulk Richardson number over the ocean. *Journal of Applied Meteorology*, *36*, 406–414.
Hahmann, A.N., Vincent, C.L., Peña, A., Lange, J., & Hasager, C. B. (2014n). Wind climate estimation using WRF model output: Method and model sensitivities over the sea. *International Journal of Climatology* (accepted for publication).
Hasager, C.B., Badger, M., Peña, A., & Larsén, X.G. (2011). SAR-based wind resource statistics in the Baltic Sea. *Remote Sensing*, *3*(1), 117–144, http://dx.doi.org/10.3390/rs3010117.
Hasager, C.B., Barthelmie, R.J., Christiansen, M.B., Nielsen, M., & Pryor, S.C. (2006). Quantifying offshore wind resources from satellite wind maps: Study area the North Sea. *Wind Energy*, *9*, 63–74.
Hasager, C.B., Nielsen, M., Astrup, P., Barthelmie, R.J., Dellwik, E., Jensen, N.O., et al. (2005). Offshore wind resource estimation from satellite SAR wind field maps. *Wind Energy*, *8*, 403–419.
Hasager, C.B., Peña, A., Christiansen, M.B., Astrup, P., Nielsen, M., Monaldo, F.M., et al. (2008). Remote sensing observation used in offshore wind energy. *IEEE Journal of Selected Topics in Applied Earth Observations and Remote Sensing*, *1*(1), 67–79.
Hasager, C.B., Stein, D., Courtney, M., Peña, A., Mikkelsen, T., Stickland, M., et al. (2013). Hub height ocean winds over the North Sea observed by the NORSEWInD lidar array: Measuring techniques, quality control and data management. *Remote Sensing*, *5*(9), 4280–4303, http://dx.doi.org/10.3390/rs509428010.3390/rs5094280.
Henderson, A., Gandoin, R., Jiménez, M.M., Yendole, H., & Méchali, M. (2013). Wind measurements campaigns offshore — How they create value for wind farms. *EWEA Offshore 2013, Frankfurt 19–21 November 2013* (http://www.ewea.org/offshore2013/conference/programme/).
Hersbach, H. (2010). Comparison of C-band scatterometer CMOD5N equivalent neutral winds with ECMWF. *Journal of Atmospheric and Oceanic Technology*, *27*, 721–736, http://dx.doi.org/10.1175/2009JTECHO698.1.
Hersbach, H., Stoffelen, A., & de Haan, S. (2007). An improved C-band scatterometer ocean geophysical model function:CMOD5. *Journal of Geophysical Research*, *112*, C03006.
Hilburn, K.A., Wentz, F.J., Smith, D.K., & Ashcroft, P.D. (2006). Correcting active scatterometer data for the effects of rain using passive radiometer data. *Journal of Applied Meteorology and Climatology*, *45*, 382–398.
Jiang, D., Zhuang, D.F., Huang, Y.H., Wang, J.H., & Fu, J.Y. (2013). Evaluating the spatio-temporal variation of China's offshore wind resources based on remotely sensed wind field data. *Renewable and Sustainable Energy Reviews*, *24*, 142–148.
Karagali, I., Badger, M., Hahmann, A., Peña, A., Hasager, C. B., & Sempreviva, A.M. (2013). Spatial and temporal variability in winds in the Northern European Seas. *Renewable Energy*, *57*, 200–210, http://dx.doi.org/10.1016/j.renene.2013.01.017.
Karagali, I., Peña, A., Badger, M., & Hasager, C. (2014). Wind characteristics in the North and Baltic Seas from the QuikSCAT satellite. *Wind Energy*, *17*(1), 123–140, http://dx.doi.org/10.1002/we.1565.
Kerbaol, V. (2007). Improved Bayesian wind vector retrieval scheme using Envisat ASAR data: principles and validation results. *Envisat Symposium, Montreux (CH), 23–27 Apr 2007, Paris*.
Koch, W. (2004). Directional analysis of SAR images aiming at wind direction. *IEEE Transactions on Geoscience and Remote Sensing*, *42*, 702–710.
Lehner, S., Horstmann, J., Koch, W., & Rosenthal, W. (1998). Mesoscale wind measurements using recalibrated ERS SAR images. *Journal of Geophysical Research - Oceans*, *103*, 7847–7856.
Liu, W.T., & Tang, W. (1996). *Equivalent neutral wind*. National Aeronautics and Space Administration, Jet Propulsion Laboratory, California Institute of Technology, National Technical Information Service, distributor.
Liu, W.T., Tang, W., & Xie, X. (2008). Wind power distribution over the ocean. *Geophysical Research Letters*, *35*(13), L13808, http://dx.doi.org/10.1029/2008GL034172.
Longépé, N., Hajduch, G., Pelich, R., Habonneau, J., & Lebras, J. -Y. (2013). SAR-based ship monitoring: Advanced methodologies with medium resolution images (from WSM ASAR to EWS/IWS S1 Mission). *ESA Living Planet Symposium, 9–13 September 2013, Edinburgh, United Kingdom*. ESA Living Planet (http://www.livingplanet2013.org/abstracts/850753.htm).
Monaldo, F.M., Thompson, D.R., Beal, R.C., Pichel, W.G., & Clemente-Colón, P. (2001). Comparison of SAR-derived wind speed with model predictions and ocean buoy measurements. *IEEE Transactions on Geoscience and Remote Sensing*, *39*, 2587–2600.
Monaldo, F.M., Thompson, D.R., Pichel, W.G., & Clemente-Colon, P. (2004). A systematic comparison of QuikSCAT and SAR ocean surface wind speeds. *IEEE Transactions on Geoscience and Remote Sensing*, *42*, 283–291.
Mortensen, N., Heathfield, D.N., Landberg, L., Rathmann, O., Troen, I., & Petersen, E.L. (2000). Wind Atlas Analysis and Wind Atlas Analysis and Application program: WAsP 7.0 Help Facility. Roskilde: Risø National Laboratory, 1–277.
Mouche, A., Collard, F., Chapron, B., Dagestad, K. -F., Guitton, G., Johannessen, J., et al. (2012). On the use of Doppler shift for sea surface wind retrieval from SAR. *IEEE Transactions on Geoscience and Remote Sensing*, http://dx.doi.org/10.1109/TGRS.2011.2174998.
Mouche, A., Hauser, D., Daloze, J. -F., & Guerin, C. (2005). Dual-polarization measurements at C-band over the ocean: Results from airborne radar observations and comparison with Envisat ASAR data. *IEEE Transactions on Geoscience and Remote Sensing*, *43*(4), 753–769, http://dx.doi.org/10.1109/TGRS.2005.843951.
Nghiem, S.V., Leshkevich, G.A., & Stiles, B.W. (2004). Wind fields over the Great Lakes measured by the SeaWinds scatterometer on the QuikSCAT satellite. *Journal of Great Lakes Research*, *30*(1), 148–165.
Nielsen, M., Astrup, P., Hasager, C.B., Barthelmie, R.B., & Pryor, S.C. (2004). *Satellite information for wind energy applications*. Roskilde, Denmark: Risø National Laboratory, 1–57.
Peña, A., & Gryning, S. -E. (2008). Charnock's roughness length model and non-dimensional wind profiles over the sea. *Boundary-Layer Meteorology*, *128*, 191–203.
Peña, A., Gryning, S.E., & Hasager, C.B. (2008). Measurements and modelling of the wind speed profile in the marine atmospheric boundary layer. *Boundary-Layer Meteorology*, *129*(3), 479–495.
Peña, A., & Hahmann, A. (2012). Atmospheric stability and turbulence fluxes at Horns Rev -an intercomparison of sonic, bulk and WRF model data. *Wind Energy*, *15*(5), 717–731, http://dx.doi.org/10.1002/we.500.
Peña, A., Hahmann, A.N., Hasager, C.B., Bingöl, F., Karagali, I., Badger, J., et al. (2011). South Baltic Wind Atlas: South Baltic Offshore Wind Energy Regions Project. *Risø-R-1775(EN), Risø National Laboratory for Sustainable Energy* (pp. 1–66). Technical University of Denmark.
Peña, A., Mikkelsen, T., Gryning, S. -E., Hasager, C.B., Hahmann, A.N., Badger, M., et al. (2012). *Offshore vertical wind shear*. DTU Wind Energy-E-Report-0005(EN), 1–116.
Petersen, E. L. (1992). Wind resources of Europe (the offshore and coastal resources). In P. H. Madsen, & P. Lundsager (Eds.), *The potential of wind farms. Proceedings of European Wind Energy Association special topics conference (1–4)*. Denmark: The Association of Danish Windmill Manufacturers (A2).
Petersen, E.L., & Troen, I. (2012). Wind conditions and resource assessment. *Energy Environment*, *1*, 206–217, http://dx.doi.org/10.1002/wene.4.
Pimenta, F., Kempton, W., & Garvine, R. (2008). Combining meteorological stations and satellite data to evaluate the offshore wind power resource of Southeastern Brazil. *Renewable Energy*, *11*, http://dx.doi.org/10.1016/j.renene.2008.01.012.
Portabella, M., & Stoffelen, A. (2002). A comparison of KNMI Quality Control and JPL Rain Flag for SeaWinds. *Canadian Journal of Remote Sensing*, *28*(3), 424–430.
Portabella, M., & Stoffelen, A. (2009). On scatterometer ocean stress. *Journal of Atmospheric and Oceanic Technology*, *26*(2), 368–382, http://dx.doi.org/10.1175/2008JTECHO578.1.
Portabella, M., Stoffelen, A., & Johannessen, J. (2002). Toward an optimal inversion method for SAR wind retrieval. *Journal of Geophysical Research-Atmospheres*, *107*(C8), 1–13, http://dx.doi.org/10.1029/2001JC000925.
Pryor, S.C., Nielsen, M., Barthelmie, R.J., & Mann, J. (2004). Can satellite sampling of offshore wind speeds realistically represent wind speed distributions? Part II Quantifying uncertainties associated with sampling strategy and distribution fitting methods. *Journal of Applied Meteorology*, *43*, 739–750.
Quilfen, Y., Chapron, B., Elfouhaily, T., Katsaros, K., & Tournadre, J. (1998). Observation of tropical cyclones by high-resolution scatterometry. *Journal of Geophysical Research*, *103*(C4), 7767–7786, http://dx.doi.org/10.1029/97JC01911.
Ricciardulli, L., & Wentz, F. (2011). Reprocessed QuikSCAT (V04) wind vectors with Ku-2011 geophysical model function. *Remote Sensing Systems, Technical Report* (http://images.remss.com/qscat/qscat_Ku2011_tech_report.pdf).
Ricciardulli, L., & Wentz, F. (2013). Challenges of integrating multiple scatterometer observations into a climate data record. *The Effect of Diurnal Variability, International Ocean Vector Wind Science Team, Kona, Hawaii, 6–8 May 2013* (http://www.coaps.fsu.edu/scatterometry/meeting/docs/2013/CalValClim/Ricciardulli_Wentz_ovwst_2013_wind_diurnal.pdf).
Sathe, A., Gryning, S. -E., & Peña, A. (2011). Comparison of the atmospheric stability and wind profiles at two wind farm sites over a long marine fetch in the North Sea. *Wind Energy*, *14*, 767–780, http://dx.doi.org/10.1002/we.456.
Sempreviva, A.M., Barthelmie, R.J., & Pryor, S.C. (2008). Review of methodologies for offshore wind resource assessment in European seas. *Surveys in Geophysics*, *29*(6), 471–497.
Stoffelen, A. (1998). Toward the true near-surface wind speed: error modeling and calibration using triple collocation. *Journal of Geophysical Research*, *103*(C4), 7755–7766.
Stoffelen, A., Vogelzang, J., & Verhoef, A. (2010). Verification of scatterometer winds. *Proc. 10th International Winds Workshop, Tokyo, Japan, 20–26 February 2010* (pp. 56). Eumetsat (http://www.Eumetsat.int/website/home/News/ConferencesandEvents/PreviousEvents/DAT_2042632.html).
Takeyama, Y., Ohsawa, T., Kozai, K., Hasager, C.B., & Badger, M. (2013a). Effectiveness of WRF wind direction for retrieving coastal sea surface wind from synthetic aperture radar. *Wind Energy*, *16*, 865–878, http://dx.doi.org/10.1002/we.1526.
Takeyama, Y., Ohsawa, T., Kozai, K., Hasager, C.B., & Badger, M. (2013b). Comparison of geophysical model functions for SAR wind speed retrieval in Japanese coastal waters. *Remote Sensing*, *5*(4), 1956–1973, http://dx.doi.org/10.3390/rs5041956.
Troen, I., & Petersen, E.L. (1989). *European wind atlas*. Roskilde, Denmark: Risø National Laboratory.
Verhoef, A., & Stoffelen, A. (2013). ASCAT coastal winds validation report. *Ocean and Sea Ice SAF Technical Note SAF/OSI/CDOP/KNMI/TEC/RP/176 on Product OSI-104, Version 1.5, KNMI* (www.knmi.nl/scatterometer/publications/pdf/ASCAT_validation_coa.pdf).
Verhoef, A., Vogelsang, J., Verspeek, J., & Stoffelsen, A. (2010). *AWDP user manual and reference guide v2.0, NWP-SAF, KNMI, de Bilt, the Netherlands*. (http://www.knmi.nl/publications/fulltexts/awdp_um_and_rg_v2_0_01.pdf).

Verspeek, J., Portabella, M., Stoffelen, A., & Verhoef, A. (2011). Calibration and validation of ASCAT winds. *OSI-SAF Technical Note SAF/OSI/KNMI/TEC/TN/163* (http://www.knmi.nl/scatterometer/publications/pdf/ASCAT_calibration.pdf).
Vogelzang, J., Stoffelen, A., Verhoef, A., & Figa-Saldana, J. (2011). On the quality of high-resolution scatterometer winds. *Journal of Geophysical Research*, *116*, http://dx.doi.org/10.1029/2010JC006640.

Web-links (all accessed latest at 5 August 2014)

Atlas of UK Marine Renewable Energy Resources (2008). ABPmer. http://www.renewables-atlas.info
ASCAT Wind Product User Manual (2012). Ocean and Sea Ice SAF, Version 1.11. http://www.knmi.nl/scatterometer/publications/pdf/ASCAT_Product_Manual.pdf
CMOD5N (2013). www.knmi.nl/scatterometer/cmod5
Crown Estate (2013). http://www.thecrownestate.co.uk/energy-infrastructure/offshore-wind-energy/our-portfolio/round-3-wind-farms/
DEA (2013). http://www.ens.dk/sites/ens.dk/files/supply/renewable-energy/wind-power/offshore-wind-power/new-offshore-wind-tenders/New%20Offshore%20Wind%20Tenders%20in%20Denmark%20FINAL.pdf
DOE (2013). http://www1.eere.energy.gov/wind/offshore_wind.html
EEA (2009b). European Environment Agency. http://www.eea.europa.eu/publications/europes-onshore-and-offshore-wind-energy-potential
EWEA (2013). http://www.ewea.org/
GWEC (2013). http://www.gwec.net
MyOcean Catalogue (2014). http://catalogue.myocean.eu.org/static/resources/myocean/pum/MYO2-OSI-PUM-012-002-V2.2.pdf
MyOcean Product User Manual (2012). http://catalogue.myocean.eu.org/static/resources/myocean/pum/MYO2-SIW-PUM-012-002-V2.1.pdf
New Scientist (2013). http://www.newscientist.com/article/dn23082-japan-to-build-worlds-largest-offshore-wind-farm.html#.UpEG7vB7zIU
NOAA (2014). http://manati.star.nesdis.noaa.gov/datasets/ASCATData.php
OSI SAF (2014). http://www.knmi.nl/scatterometer/osisaf/
RSS (2014). http://www.remss.com/